Published in final edited form as:
Nat Immunol. 2018 September ; 19(9): 932–941. doi:10.1038/s41590-018-0184-1.

Control of inducible gene expression links cohesin to hematopoietic progenitor self-renewal and differentiation

Sergi Cuartero[1], **Felix D. Weiss**[#1], **Gopuraja Dharmalingam**[#3], **Ya Guo**[#1], **Elizabeth Ing-Simmons**[#1,2,12], **Silvia Masella**[4], **Irene Robles-Rebollo**[1], **Xiaolin Xiao**[3], **Yi-Fang Wang**[3], **Iros Barozzi**[4,5], **Dounia Djeghloul**[1], **Mariane T. Amano**[1,12], **Henri Niskanen**[6], **Enrico Petretto**[3,7], **Robin D. Dowell**[8], **Kikuë Tachibana**[9,12], **Minna U. Kaikkonen**[6], **Kim A. Nasmyth**[9], **Boris Lenhard**[2], **Gioacchino Natoli**[10,11], **Amanda G. Fisher**[1], and **Matthias Merkenschlager**[1,14]

[1]Lymphocyte Development Group, Epigenetics Section, MRC London Institute of Medical Sciences, Institute of Clinical Sciences, Faculty of Medicine, Imperial College London, London, UK [2]Computational Regulatory Genomics Group, Integrative Biology Section, MRC London Institute of Medical Sciences, Institute of Clinical Sciences, Faculty of Medicine, Imperial College London, London, UK [3]MRC London Institute of Medical Sciences, Institute of Clinical Sciences, Faculty of Medicine, Imperial College London, London, UK [4]Department of Experimental Oncology, European Institute of Oncology, Milan, Italy [5]Department of Surgery and Cancer, Department of Medicine, Imperial College London, London, UK [6]A. I. Virtanen Institute for Molecular Sciences, University of Eastern Finland, Kuopio, Finland [7]Cardiovascular and Metabolic Disorders, Duke-NUS Medical School, Singapore [8]BioFrontiers Institute and Department of Molecular, Cellular and Developmental Biology, University of Colorado, Boulder,

[14]Address correspondence to matthias.merkenschlager@lms.mrc.ac.uk.
[12]Present addresses: Max Planck Institute for Molecular Biomedicine, Muenster, Germany (LIS), Hospital Sírio-Libanês, Sao Paulo, Brazil (MTA), Institute of Molecular Biotechnology of the Austrian Academy of Sciences, Vienna Biocenter, Vienna, Austria (KT)

Reporting summary
Further information on experimental design is available in the Nature Research Reporting Summary linked to this article.

Data availability. The data generated for this study has been deposited at the Gene Expression Omnibus (GEO) under accession GSE108599. The data supporting the findings of this study are available from the corresponding author upon reasonable request.

Code availability. All code used in this study is available from the authors.

Accession codes. The data generated for this study has been deposited at the Gene Expression Omnibus (GEO) under accession GSE108599

Contributions
S.C. conceived and designed the study, performed most experiments including those based on genetic Rad21 deletion, analysed data, designed figures and contributed to writing the manuscript, F.D.W. performed experiments based on RAD21-TEV cleavage and contributed to writing the manuscript, G.D., X.X., and Y.-F.W. analysed data, Y.G. performed and analysed 4C experiments, E.I.-S. analysed data, designed figures and contributed to writing the manuscript, S.M. performed 5C experiments, I.R.-R. performed and analysed immunofluorescence experiments, designed figures and contributed to writing the manuscript, I.B. analysed data and contributed to writing the manuscript, D.D. designed and performed flow cytometry experiments, M.T.A. performed experiments, H.N. designed and performed GRO-seq experiments, E.P. and B.L. designed and supervised data analysis, R.D.D. conceived and performed analysis of enhancer TSSs, K.T. and K.A.N. generated and provided essential reagents, M.U.K. designed and supervised GRO-seq experiments, G.N. designed and supervised 5C experiments and contributed to writing the manuscript, A.G.F. contributed to study design and writing the manuscript, M.M. conceived and designed the study, wrote the manuscript, made figures, and supervised performing of experiments. All authors discussed the results and commented on the manuscript.

Competing financial interests. The authors declare that they have no conflicts of interest.

Europe PMC Funders Author Manuscripts

CO, USA [9]Department of Biochemistry, University of Oxford, Oxford, UK [10]Humanitas Clinical and Research Center, Milan, Italy [11]Humanitas University, Milan, Italy

[#] These authors contributed equally to this work.

Europe PMC Funders Author Manuscripts

Abstract

Cohesin is important for 3-dimensional (3D) genome organization. Nevertheless, even the complete removal of cohesin has surprisingly little impact on steady-state gene transcription and enhancer activity. Here we show that cohesin was required for the core transcriptional response of primary macrophages to microbial signals, and for inducible enhancer activity that underpins inflammatory gene expression. Consistent with a role of inflammatory signals in promoting myeloid differentiation of hematopoietic stem and progenitor cells (HPSCs), cohesin mutations in HSPCs led to reduced inflammatory gene expression, and increased resistance to differentiation-inducing inflammatory stimuli. These findings uncover an unexpected dependence of inducible gene expression on cohesin, link cohesin with myeloid differentiation, and may help explain the prevalence of cohesin mutations in human acute myeloid leukemia.

Introduction

Cohesin is a multiprotein complex that cooperates with the sequence-specific DNA binding protein CTCF in forming key features of 3D genome organization such as topologically associated domains (TADs), contact domains and chromatin loops. These features spatially compartmentalize genes and enhancers in interphase1–7 and are believed to facilitate preferential interactions between promoters and enhancers located in the same domain5,6,8–11. Removal of architectural proteins, CTCF binding sites, or domain boundaries weakens insulation between domains, thus exposing genes to regulatory elements in neighboring domains and potentially perturbing gene regulation5,7,12–17. However, with few notable exceptions of specific deregulated genes12–17or DNA damage responses due to essential cohesin functions in the cell cycle18,19, loss of cohesin or CTCF have shown limited impact on transcriptional control2,4, chromatin marks, or enhancer states3,7,20. Even the complete removal of cohesin or CTCF, which abrogates the formation of CTCF–cohesin-based chromatin loops and substantially weakens TADs2,4, did not result in clear gene regulatory phenotypes. This finding raised concerns whether current models overstate the significance of spatial genome compartmentalization for gene regulation. However, it is still unclear to what extent such limited impact of cohesin on gene regulation also applies to inducible responses, such as the core myeloid inflammatory gene expression program21–25. Here, hundreds of genes and thousands of gene regulatory elements are rapidly activated in a highly coordinated fashion, likely imposing an extraordinary level of regulatory requirements21–25.

In addition to its role in genome compartmentalization in interphase, cohesin is essential for genome integrity in cycling cells26. Because of this role, it may seem counterintuitive that cohesin mutations are frequently found in cancers, including acute myeloid leukemia27–29(AML). However, partial loss of cohesin is compatible with cell proliferation, and drives

increased self-renewal of hematopoietic stem and progenitor cells30–34 (HSPCs). As increased self-renewal can facilitate leukemic transformation, it is important to elucidate the mechanisms that link cohesin to pathways that regulate the balance between self-renewal and differentiation. Defining these mechanisms in HSPCs with reduced cohesin function is complicated, as it is unclear whether changes in gene expression and chromatin state are cause or consequence of increased self-renewal and reduced differentiation30–34.

To address these issues, we engineered mature, non-proliferating macrophages that can be depleted of cohesin in an inducible fashion after a normal history of differentiation. We show that cohesin was critically required for inflammatory gene expression in macrophages, HSPCs, and in primary human AML cells. As inflammatory signals regulate HSPC self-renewal and myeloid differentiation35–42, our findings provide a mechanistic link between cohesin, inflammation and AML.

Results

Cohesin controls inflammatory gene expression in AML

To explore the role of cohesin in AML, we examined the correlation between cohesin mutations and gene expression by analyzing RNA-seq data for 173 primary AML samples compiled by The Cancer Genome Atlas28 (TCGA). Twenty-three had missense or truncating mutations in the genes encoding the cohesin subunits RAD21, SMC3, SMC1A or STAG2 (Fig. 1a). Gene set enrichment analysis (GSEA) showed that inflammatory genes were the most strongly downregulated gene set in AML with cohesin mutations, closely followed by interferon-responsive genes (Fig. 1b; FDR < 0.001). Genes involved in the interferon-α (IFN-α), IFN-γ, and tumor necrosis factor (TNF) signaling pathways were similarly downregulated in cohesin-mutated AML (Fig. 1c).

AML samples of different French-American-British (FAB) subtypes43 had characteristic patterns of inflammatory gene expression (not shown). Among the 37 AML samples classified by TCGA as FAB M2, 10 had cohesin mutations, providing sufficient power to compare gene expression within this subtype. GSEA identified inflammatory genes and genes involved in the IFN-α and IFN-γ pathways as the top 3 downregulated gene sets in FAB M2 AML with cohesin mutations (FDR = 0; Fig. 1d), linking reduced inflammatory gene expression to impaired cohesin function, rather than AML subtype. This analysis of TCGA samples suggests a previously unrecognized role for cohesin in the regulation of inflammatory genes in human AML.

Inducible genes are sensitive to cohesin dosage

We next analyzed the impact of cohesin on inflammatory gene expression in primary mouse macrophages. These mature, quiescent myeloid cells are suitable for mechanistic studies of gene expression21–25. To uncouple cohesin deletion from myeloid differentiation we allowed myeloid progenitors to differentiate into mature macrophages, and subsequently deleted the gene encoding the essential cohesin subunit RAD21 (Supplementary Fig. 1a,b). Floxed *Rad21* alleles were removed within 24 h of inducible ERt2Cre activation by 4-hydroxy-tamoxifen (4-OHT), and RAD21 protein expression declined gradually over 2-3

days (Supplementary Fig. 1b-e). This approach allowed homozygous cohesin deletion, as the cell cycle functions of cohesin are essential in cycling but not in quiescent cells17 (Supplementary Fig. 1d,f). The use of quiescent cells also precludes any selective expansion of immature cells (as seen in HSPCs with reduced cohesin function30–34), and thereby enables like-for-like comparisons of gene expression and chromatin state between control and cohesin-deficient cells.

We used RNA-seq to profile gene expression in *Rad21*-deleted macrophages containing less than 15% residual RAD21 protein (Fig. 2a). As expected2,4,7,17, the overall impact on gene expression was limited. Approximately 10% of constitutively expressed genes were up- or downregulated (adj. $P < 0.05$; Fig. 2b). However, genes that are inducible by inflammatory signals23 (Fig. 2b) were more severely affected by the loss of cohesin than constitutively expressed genes. Over 50% of inducible genes were deregulated at baseline (Fig. 2c).

In macrophages, activation of Toll-like receptor 4 (TLR4) by the bacterial cell wall component lipopolysaccharide (LPS) triggers a program of inducible gene expression23, but not proliferation. Transcription factor and cytokine genes are activated early, and cytokines (notably IFN-β) trigger the auto- and paracrine induction of secondary response genes23 (Fig. 2b). This program was curtailed in *Rad21*-deleted macrophages. The frequency of deregulated inducible genes progressively increased with time after LPS (Fig. 2c,d). Deregulated inducible genes23 included genes classified as IFN-dependent24 and, albeit to a lesser extent, IFN-independent genes24. Specifically, 88% of IFN-dependent inducible genes and 68% of IFN-independent inducible genes were deregulated at adj. $P < 0.05$ 8 h after LPS treatment.

Deregulation of inducible genes was profound not only in terms of the frequency of deregulated genes, but also in terms of the fold-change (Fig. 2e). For example, 32% of inducible genes but only 5% of constitutive genes were deregulated 4-fold or more 8 h after LPS stimulation (not shown). The transcription factor NF-κB is a key regulator of inducible genes in macrophages21–25. After TLR4 activation by LPS, NF-κB was predominantly nuclear in *Rad21*-deleted as well as wild-type macrophages (Supplementary Fig. 1g). The deregulation of inducible genes was therefore not explained by non-responsiveness of *Rad21*-deficient macrophages to LPS.

Inducible macrophage genes are mostly pro-inflammatory23–25 and genes related to the inflammatory response were predominantly downregulated in *Rad21*-deleted macrophages (FDR = 0.0; Fig. 2f). These changes in gene expression affected the secretion of inducible cytokines by *Rad21*-deleted macrophages. Of 26 LPS-responsive cytokines tested, 16 were deregulated, and 13 were decreased, including IFN-β, IL-6 and TNF (Supplementary Fig. 1h). Analysis of heterozygous $Rad21^{+/-}$ macrophages (which retained 77 ± 6% of RAD21 protein expression compared to $Rad21^{+/+}$ macrophages, not shown) indicated that partially reduced cohesin function was sufficient to impair inducible gene expression (Fig. 2g).

Immediate impact of acute cohesin depletion

Because RAD21 protein abundance declined gradually after genetic deletion of *Rad21* (Supplementary Fig. 1c), cells were in a cohesin-depleted state for 24 to 48 h prior to RNA-

seq analysis. It was therefore unclear to what extent inducible gene expression was under the direct control of cohesin. To address this question, we developed an experimental system for acute cohesin depletion based on *Rad21* alleles engineered by insertion of cleavage sites for the Tobacco Etch Virus (TEV) protease into the endogenous locus44. Fetal liver cells expressing TEV-cleavable RAD21 (RAD21-TEV) as their sole source of RAD21 protein were transduced with a cytoplasmic TEV-ERT2 fusion construct, and differentiated into mature, quiescent macrophages. Addition of the ERt2 ligand 4-OHT released TEV-ERT2 to the nucleus, and RAD21-TEV protein was rapidly degraded (Fig. 3a). RNA-seq 8 h after 4-OHT showed that acute depletion of cohesin resulted in the deregulation of 1016 genes (adj. $P < 0.05$ based on DEseq2 analysis of 3 RNA-seq replicates). The majority of these genes (557 of 1016 or 55%) were also deregulated by *Rad21* deletion ($P < 2.22e-16$, odds ratio = 2.65, Fisher's exact test). Acute depletion of cohesin deregulated a significantly higher fraction of inducible than constitutive genes (Fig. 3b, $P < 2.22e-16$, odds ratio = 4.44). Deregulated genes were enriched for terms including signaling (adj. $P = 1.33e-08$), inflammatory response (adj. $P = 7.93e-07$), immune system (adj. $P = 9.23e-06$), and inflammation mediated by chemokine and cytokine signaling (adj. $P = 2.44e-08$). A 2 h pulse of LPS further deregulated inducible genes in 4-OHT-treated RAD21-TEV macrophages ($P < 2.22e-16$, odds ratio = 3.54; Fig. 3b). Inducible genes23 deregulated immediately after RAD21-TEV cleavage included both IFN-dependent24 and IFN-independent genes (Fig. 3b). Inflammatory response genes were preferentially downregulated (Fig. 3c). Most inducible genes23 that were downregulated by acute cohesin depletion were also downregulated by *Rad21* deletion (44 of 69, 64% at baseline, $P < 0.0005$, odds ratio = 2.60; and 99 of 127, 78%, after 2 h LPS, $P < 9.17e-10$, odds ratio = 3.94, Fisher's exact test). Transcripts downregulated immediately after cohesin cleavage in RAD21-TEV macrophages included regulators of inducible gene expression, such as transcription factors (*Fos, Jun, Irf2, Myc, Ets2, Prdm1/Blimp1, Egr2, Cebpa, Cebpb*), inflammatory cytokines (*Il1b*), chemokines (*Ccl3, Ccl7, Ccl9*), chemokine receptors (*Ccr1, Ccr3, Ccr5*), and receptors for inflammatory mediators (*Ifnar1, Ifnar2, Ifngr1*). Hence, inducible genes were under the immediate control of cohesin.

Restricted enhancer dynamics in cohesin-deficient macrophages

The macrophage enhancer landscape is dynamically reconfigured in response to activation21,22. Constitutive, activation-inducible, and activation-repressed enhancers have been characterized based on acetylation of lysine 27 of histone H3 (H3K27ac), H3K4me1, and binding of the transcription factor PU.1 at promoter-distal sites22. We found that *Rad21* deletion did not affect H3K27ac at the great majority (97.2%) of constitutively active enhancers22 (DEseq2 adj. $P < 0.05$, Fig. 4). In contrast, H3K27ac was broadly deregulated at LPS-inducible enhancers22 (2.6% of constitutive versus 24.8% of inducible enhancers, Fig. 4, Supplementary Fig. 2a) and LPS-repressed enhancers22 (15.6%, $P < 0.05$, Supplementary Fig. 2a). In addition to H3K27ac, active enhancers are characterized by increased chromatin accessibility and enhancer transcription. We assessed enhancer accessibility by ATAC-seq (Supplementary Fig. 2b) and enhancer transcription by GRO-seq (Supplementary Fig. 2c,d) and confirmed that the activation of inducible enhancers was impaired in cohesin-deficient macrophages. We conclude that cohesin controls inducible gene expression and enhancer dynamics in macrophages.

Genomic organization of deregulated genes and enhancers

Deregulated inducible genes23 were enriched near deregulated inducible enhancers22 (adj. $P < 0.005$ by nearest neighbor analysis, odds ratio = 2.11 in resting macrophages; adj. $P =$ 4.05e-6, odds ratio = 1.70 after 6 h LPS for enhancers and 8 h LPS for transcripts). Deregulated genes and enhancers were significantly enriched within the same TADs (adj. P = 2.70e-111, odds ratio = 7.23 for H3K27ac deregulated enhancers; adj. $P =$ 4.47e-43, odds ratio = 5.02 for GRO-seq-deregulated enhancers, Supplementary Fig. 3a). Coherence between gene expression and enhancer states (Supplementary Fig. 3a) is illustrated by domains that harbor downregulated enhancers and clusters of downregulated chemokine genes45 (Supplementary Fig. 3b). To assess LPS-induced changes in chromatin contacts we applied serial 5C analyses of a ~5Mb region rich in inducible genes and enhancers in wild-type macrophages. Most chromatin contacts remained unchanged in response to LPS (fold-change < 2, Supplementary Fig. 3b). While average interactions between inducible promoters and enhancers did not increase significantly in response to LPS (Supplementary Fig. 3c), 4C analysis suggested that a subset of chromatin contacts at the inducible *Egr2* locus were reconfigured in response to LPS (Supplementary Fig. 4a). Consistent with known cohesin functions1,3,4,8, local chromatin contacts appeared reduced in *Rad21*-deleted macrophages at the *Egr2* locus (Supplementary Fig. 4b) and after acute RAD21 depletion by TEV cleavage at the *Egr2*, *Ifnar1*, and *Cebpb* loci (Supplementary Fig. 4c).

Chromatin accessibility of inducible enhancers

Global assessment of chromatin accessibility by ATAC-seq identified similar numbers of accessible sites in unstimulated wild-type and *Rad21*-deleted macrophages. In response to LPS, chromatin accessibility increased in wild-type but not in cohesin-deficient macrophages as judged by the number of ATAC-seq peaks, and the percentage of reads in peaks (Supplementary Fig. 5a). This difference in accessibility was pronounced at the transcription start sites (TSS) of LPS-inducible enhancers46 (Supplementary Fig. 5b). As cohesin can facilitate chromatin remodeling and accessibility47–50 we explored the relationship between cohesin binding and enhancer accessibility. Very few inducible enhancers acquired new RAD21 ChIP-seq peaks in response to LPS, but ~1/3 of inducible enhancers showed increased RAD21 ChIP-seq reads (not peaks) in wild-type macrophages. Activation-induced cohesin binding in wild-type macrophages was not predictive of enhancer failure after *Rad21* deletion ($P = 0.67$, odds ratio = 0.96). These findings suggested that factors other than RAD21 binding contributed to enhancer failure in *Rad21*$^{-/-}$ macrophages.

Failed enhancers have ISRE or IRF-PU.1 motifs

To understand enhancer deregulation in cohesin-deficient macrophages, we focused on inducible enhancers that showed LPS-induced upregulation of H3K27ac ($P < 0.05$ and FC ≥ 1.5) and active enhancer transcription in wild-type macrophages. We classified inducible enhancers into those that remained intact versus those that failed to upregulate H3K27ac in *Rad21*$^{-/-}$ macrophages (adj. $P < 0.05$), and compared transcription factor motifs at their transcription start sites46. Intact enhancers were enriched for NF-κB ($P =$ 10-65 for H3K27ac, $P =$ 10-251 for GRO-seq) and NFAT motifs ($P =$ 10-15 for H3K27ac, $P =$ 10-47

for GRO-seq). Failed enhancers were instead enriched in IFN-stimulated response elements (ISRE, targeted by STAT and IRF, $P = 10\text{-}14$ for H3K27ac, $P = 10\text{-}49$ for GRO-seq) and IRF-PU.1 composite motifs ($P = 10\text{-}19$ for H3K27ac, $P = 10\text{-}9$ for GRO-seq; Fig. 5a). ATAC-seq showed that chromatin accessibility of inducible enhancers with ISRE or IRF-PU.1 motifs was profoundly reduced in *Rad21*$^{-/-}$ macrophages, more so than accessibility of inducible enhancers with NFAT or NF-κB motifs (Fig. 5b). Inducible enhancers with ISRE or IRF-PU.1 motifs were more likely to fail ($P = 10\text{-}6$, odds ratio = 8.94), while inducible enhancers with NF-κB or NFAT motifs were less likely to fail ($P = 0.003$, odds ratio = 0.55; Table 1). Consistent with these findings, RNA-seq and quantitative RT-PCR showed reduced expression of the LPS-inducible transcription factors *Stat1, Stat2,* and *Irf7* expression in *Rad21*-deleted macrophages (Fig. 5c). These findings suggest that reduced expression of transcription factors contributed to enhancer failure in *Rad21*$^{-/-}$ macrophages.

Partial rescue of inducible genes and enhancers by IFN

The organization of inducible gene expression is hierarchical (Supplementary Fig. 6a), as early events, including the induction of transcription factors and cytokines, are required for the appropriate regulation of downstream genes23–25. In hierarchical networks, information propagates from a small number of upstream nodes, e.g. TLRs or IFN receptors, to numerous downstream targets (Supplementary Fig. 6a). This strategy is vulnerable, as failure of early events can cause widespread defects51. We considered whether the organization of inducible gene expression in macrophages might compound the deregulation of inflammatory gene expression in cohesin-deficient cells. Our data implicate the IFN pathway as a key intermediate. First, inducible enhancers targeted by the IFN signaling pathway components STAT and IRF are prone to fail in cohesin-deficient macrophages. Second, IFN signaling genes are deregulated by acute cohesin depletion. Based on these observations, we tested the impact of exogenous IFN-β on inducible gene expression. IFN-β induced *Stat1, Stat2,* and *Irf7* expression, and significantly reduced the difference in the expression of these mediators between *Rad21*-deleted and wild-type macrophages (Fig. 6a).

We next assessed the impact of IFN on failed inducible enhancers with ISRE or IRF-PU.1 motifs and/or ChIP-seq evidence for STAT binding. Treatment of control and *Rad21*-deleted macrophages with IFN-β or IFN-γ followed by ChIP-PCR partially rescued H3K27ac (Fig. 6b). This result shows that cytokines and the transcription factors they regulate can promote enhancer activation in the absence of cohesin (Supplementary Fig. 5c).

Finally, we tested the global impact of IFN priming on LPS-inducible gene expression in *Rad21*-deleted macrophages by RNA-seq (Fig. 6c) and found partial rescue of early and late inducible gene classes23. Rescue included a subset of domains with deregulated gene expression, as illustrated for clusters of *Slfn*, *Ccl*, *Gbp* and *Lrrc* genes (Fig. 6d). This rescue is most likely explained by the shared regulatory requirements of gene duplicates contained within these clusters45.

At the genomic level, cohesin-dependent genes are enriched for cohesin binding17 as well as proximity to enhancers and super-enhancers4,7,20. These features are evident for both constitutive and inducible genes deregulated by acute degradation of RAD21-TEV (Supplementary Fig. 6b), as illustrated by the IFN receptor genes *Ifnar1* and *Ifnar2*

(Supplementary Fig. 6c). Acute cohesin depletion in RAD21-TEV macrophages preferentially deregulated cohesin-bound genes close to enhancers and super-enhancers (Supplementary Fig. 6d). The deregulation of inducible genes became more extensive after prolonged cohesin depletion: In response to acute cohesin depletion in RAD21-TEV macrophages, 25% of inducible genes were deregulated at baseline. The fraction of deregulated inducible genes increased to > 50% after 1 to 2 days of cohesin depletion in *Rad21*-deleted macrophages. Similarly, 39% of inducible genes were deregulated after 2 h LPS activation of acutely cohesin-depleted macrophages, which increased to 60 to 80% in LPS-stimulated macrophages 1 to 2 days after cohesin depletion. As deregulation spread to include most inducible genes in *Rad21*-deleted macrophages, it was no longer focused on enhancer-proximal and cohesin-bound genes (Supplementary Fig. 6d). These findings are consistent with the logic of the inducible gene expression network discussed above.

Overall, inducible genes were highly enriched for genomic proximity to enhancers, inducible enhancers, and super-enhancers ($P < 2.2e\text{-}16$; Supplementary Fig. 6e) as a genomic correlate of cohesin-dependence4,7,20. Hence, inducible gene expression is vulnerable to cohesin depletion at 2 distinct levels; the cohesin-dependence of its constituent components, and the topology of the inducible gene expression network.

Cohesin controls inflammatory gene expression in HSPCs

To address the relationship between cohesin, inflammatory gene expression and differentiation, we extended our analysis to HSPCs. Inflammatory signals cause gene expression changes in HSPCs35–42. Conversely, HSPCs contribute to the production of inflammatory cytokines that regulate HSPC self-renewal and differentiation40,42,52. Inflammatory signals promote myeloid differentiation at the expense of HSPC self-renewal35–42, and HSPCs with reduced cohesin function display enhanced self-renewal in serial in vitro colony-forming assays30–32 and in vivo competitive reconstitution experiments32. We therefore examined gene expression in lineage negative, $Sca1^+$, $c\text{-}Kit^+$ (LSK) progenitors with reduced cohesin function following *Stag2* RNAi in vivo31 and found a notable downregulation of inflammatory genes at baseline (Fig. 7). Equivalent results were seen in progenitors with reduced *Smc1a* 31 and *Smc3* 32 expression (not shown). Re-analysis of published gene expression data31,32,53 confirmed that pro-inflammatory pathways that were downregulated in cohesin-deficient HSPCs31,32 were reciprocally upregulated in HSPCs exposed to chronic *M. avium* infection53 ($P = 5.9e\text{-}28$, odds ratio = 7.59, Table 2). These findings link cohesin to inflammatory gene expression in HSPCs.

HSPCs respond to cohesin-dependent inflammatory signals

To evaluate the biological impact of cohesin-dependent cytokine secretion, we isolated LSKs by flow cytometry (Fig. 8a). Seven of 10 stem cell genes tested showed reduced expression in LSKs exposed to medium conditioned by LPS-pulsed wild-type macrophages (Fig. 8b). Medium conditioned by LPS-pulsed *Rad21*-deleted macrophages had markedly less impact on stem cell gene expression (Fig. 8b). Common myeloid progenitors (CMPs) and granulocyte-macrophage (GMP) progenitors upregulated the expression of the myeloid differentiation markers CD11b and CD16 in response to medium conditioned by wild-type

macrophages, but medium conditioned by *Rad21*-deleted macrophages was less effective (Fig. 8c). These data show that HSPCs are sensitive to cohesin-dependent inflammatory signals.

Cohesin controls HSPC responses to inflammatory stimuli

Finally, we asked how cohesin mutations affect the sensitivity of HSPCs to inflammatory signals. In response to the pro-inflammatory signal LPS, *Rad21*$^{+/-}$ LSK showed significantly lower inflammatory gene expression than wild-type LSK (Fig. 8d). LPS reduced the expression of stem cell genes in wild-type LSKs, but stem cell gene expression was markedly more robust to LPS exposure in *Rad21*$^{+/-}$ LSKs (Fig. 8e). We conclude that cohesin connects inflammation with self-renewal and differentiation by controlling the expression of inflammatory genes by HSPCs at baseline and in response to inflammatory stimuli, and the sensitivity of HSPCs to inflammatory signals.

Discussion

Depletion of cohesin or CTCF disrupts key features of 3D chromatin organization, but in previous studies had limited impact on the maintenance of gene expression and chromatin modifications3,4,7,20. These findings called into question the significance of genome folding for the regulation of gene expression, chromatin state and enhancer activity. Here we show that cohesin was critically required for inducible gene expression and enhancer dynamics in primary myeloid cells. This indicates an important role for cohesin in the transition from a resting to an activated state, and suggests that the impact of cohesin on gene expression may have been underestimated by studies confined to cell lines under steady-state conditions.

Inducible genes are subject to regulation by a complex network of enhancers21,22 and our data show that inducible genes are significantly enriched in the vicinity of enhancers and super-enhancers. Enhancer interactions are altered in the absence of cohesin4,20, consistent with models where cohesin-dependent chromatin contacts facilitate enhancer-promoter contacts and counteract the segregation of chromatin regions according to chromatin state3,4,7,20. These findings offer an explanation for the enrichment of inducible genes among immediate cohesin-regulated genes. The organization of the inducible gene expression network is hierarchical, and the expression of secondary response genes depends on inducible transcription factors and cytokines that act in an auto-and paracrine fashion23,25,54. This regulatory logic and the cohesin-dependence of inducible genes, including IFN receptors and IFN-regulated transcription factors, render inducible gene expression particularly vulnerable to disruption by the loss of cohesin. In support of this model, exogenous provision of inducible cytokines partially rescued inducible genes and enhancer dynamics in the absence of cohesin.

Cohesin is required for cell proliferation26, yet many cancers accumulate cohesin mutations27,28. These findings are reconciled by data that the amount of cohesin present in normal cells is in excess of what is required for sister chromatid cohesion55. Modest reductions in cohesin function affect the development of multiple organ systems in humans56, suggesting that the correct expression of developmental genes is highly sensitive

to cohesin dosage. In HSPCs, reduced cohesin function tilts the balance between self-renewal and differentiation, and allows increased proliferation of immature progenitors30–34. Here we provide an explanation for this finding, by demonstrating that HSPCs with reduced cohesin function show reduced inflammatory gene expression, and increased resilience to the differentiation-inducing effect of inflammatory signals. Importantly, we find that cohesin mutations impair the expression of inflammatory genes also in human AML. The regulation of inflammatory gene expression and the sensitivity to inflammatory signals provide a mechanistic link between cohesin and myeloid differentiation35–42. As inflammatory mediators control the self-renewal and differentiation of HSPCs in an auto- and paracrine fashion35–42, this model suggests a mechanism for how cohesin mutations may favour self-renewal, delay differentiation, and provide a selective advantage in AML. Our data establish precedent for cohesin-dependence of gene regulatory networks. Similar mechanisms may operate in human development, where cohesin mutations disrupt multiple systems56, and in cancers other than AML.

Methods

Mice and cell culture

Mouse work was performed according to the Animals (Scientific Procedures) Act under the authority of project licence PPL70/7556 issued by the Home Office, UK following approval by the Imperial College London ethics review board. Bone marrow cells from *Rosa*26-ERt2Cre57 *Rad21*$^{WT/WT}$ or *Rad21*$^{lox/lox}$ mice17 were cultured in complete DMEM medium (10% FCS, 1% Penicillin-Streptomycin, 0.05 mM β-mercaptoethanol, 2 mM L-glutamine, 1 mM Na Pyruvate), 20% L929-conditioned media. Cre was induced on day 4 by 200 nM 4-hydroxy tamoxifen (Sigma-Aldrich H7904). Macrophages were stimulated on day 7 with 10 ng/ml of LPS from *Salmonella typhosa* (Sigma-Aldrich L7895), where indicated after priming for 24 h with 10 ng/ml mouse IFN-γ (Invitrogen PMC4031) or 100 U/ml mouse IFN-β (Chemicon IF011).

For TEV cleavage of RAD21 protein, macrophages were isolated from E14 *Rad21*$^{tev/tev}$ fetal livers44 and plated in complete IMDM with 20% L929-conditioned media. Two days later, 4×10^6 cells were resuspended in 2 ml retroviral supernatant, 4μg/ml polybrene, and centrifuged at (1250g, 90 min, 37ºC). After 8 to 10 days, 500 nM 4-hydroxy tamoxifen or carrier (ethanol) was added for 8 h. Where indicated, cells were treated with LPS (2 h, 10 ng/ml). The top 20-30% GFP-expressing cells were sorted for RNA and protein analysis.

LSKs, CMPs and GMPs were sorted from bone marrow depleted of lineage markers (CD4, CD8, B220, CD19, NK1.1, CD11b, Ter119, GR-1, Miltenyi 130-048-102 streptavidin-beads). Cells were stained with Sca-1-BV510 (BD 565507), cKit-PE (eBioscience 12-1171-81), CD16-APC (eBioscience 17-0161-81), and CD34-FITC (eBioscience 11-0341-81) and remaining lineage-positive cells were gated out using biotinylated streptavidin-eFluor 450 (eBioscience 48-4317-82). *Rad21*$^{+/-}$ bone marrow was derived from mice with a germline deletion of one *Rad21* allele. Sorted populations were cultured in complete DMEM, 100 ng/ml recombinant mouse SCF (Peprotech 250-03). Where indicated, we added filtered media conditioned for 24 h by macrophages that had been LPS-activated for 60 minutes and then washed.

FACS analysis

Macrophages were stained with CD11b-FITC (BD 561688), F4/80-PE (eBioscience 12-4801-80) with anti-Mouse TCR Vα 11.1/11.2-FITC and Vα2-PE as isotype controls. CMPs and GMPs were analysed by Sca-1-FITC (Biolegend 122505), cKit-Alexa Fluor 700 (eBioscience 56-1172-80), CD11b-APC-Cy7 (BD 557657) and CD16-BV605 (BD 563006).

TEV protein cloning and virus production

TEV cDNA was amplified from the pRNA vector and a v5 epitope tag (GKPIPNPLLGLDST) was inserted upstream of the TEV sequence. ERt2 and v5-TEV were fused by PCR using primers with XhoI and EcoRI sites and cloned into the XhoI-EcoRI site upstream of an internal ribosome entry site into pMSCV-IRES-GFP58. Retrovirus was generated as described58.

Immunoblots and antibody arrays

RAD21 (Abcam ab992), β-Actin (Santa Cruz sc-69879), c-Myc (Santa Cruz sc-40 9E10) and GAPDH (Abcam ab8245) were used for immunoblots. Cytokine arrays (R&D ARY006) and IFN-β ELISA (RnD 42400-1) were performed following manufacturer's instructions using supernatant from macrophages collected 8 h after LPS stimulation (10 ng/ml). Immunoblots and antibody arrays were imaged using an Odyssey CLx instrument (LI-COR).

Immunofluorescence

Macrophages were seeded at 2×10^5 per coverslip, treated with LPS (10 ng/ml), fixed with formaldehyde (4%, 15 min), permeabilized with Triton X-100 (0.1%, 10 min), blocked with goat serum (10%, 30 min), and incubated with 1:100 p65 antibody (Abcam ab7970) in 10% serum for 1 h, followed by 1:750 goat anti-rabbit Alexa Fluor 488 (Invitrogen A11034) and mounting in ProLong Gold Antifade Mountant with DAPI (Invitrogen).

Image acquisition and analysis

Four 3D stacks were imaged per sample with a Leica SP8 microscope (between 113 to 340 cells imaged per sample, 1024 × 1024 pixels per image, with a pixel size of 0.2027 × 0.2027 μm, ×40 oil objective). Maximum projections were analyzed in CellProfiler59 using a pipeline that identifies nuclei (IdentifyPrimaryObjects) and the cell outline (IdentifySecondaryObjects) to determine the correlation between the DAPI signal and p65 fluorescence. Correlations > 0.5 were considered indicative of nuclear translocation.

RT-qPCR

RNA was extracted with Trizol (Ambion) or RNA-bee (Amsbio) from macrophages and PicoPure kit (Applied Biosystems KIT0204) from progenitors. cDNA synthesis used Superscript reverse transcriptase (Invitrogen) and qPCR with IQ SYBR Green Supermix (Bio-Rad) and a CFX Real-time PCR system (Bio-Rad). Primers are listed in Supplementary Table 1. Ct values were normalized to *Actb* and *Hprt*.

RNA-seq

RNA sequencing was performed from 3 biological replicates per condition. RNA from 2 × 10^6 cells was extracted with RNeasy minikit and using Qiashredder (Qiagen). RNA was assessed for quality (Bioanalyzer, Agilent) and quantity (Qubit, Invitrogen). ERCC RNA Spike-Ins (Ambion) were added, and strand-specific libraries prepared from 750 ng of total RNA using TruSeq Stranded total RNA Kit (Illumina RS-122-2201). RNA from liver-derived macrophages was purified by PicoPure RNA Isolation kit (Applied Biosystems KIT0204) and 100 ng were used to prepare libraries using the NEBNext® Ultra™ II Directional RNA Library Prep Kit for Illumina. Library quality and quantity were assessed on a Bionalyzer and Qubit respectively. Libraries were sequenced on an Illumina Hiseq2500 (v4 chemistry), generating > 40million paired end 100-bp reads per sample.

GRO-seq

GRO-Seq libraries21 were prepared from two biological replicates per condition from 5 × 10^6 cells. After nuclear run-on, RNA was extracted using Trizol (Ambion), treated with Turbo DNAse (Ambion AM1907), fragmented (Ambion AM8740), purified on P-30 columns (Bio-Rad 732-6250), dephosphorylated with PNK (New England Biolabs Y904L) and purified using anti-BrdU beads (SantaCruz sc-214314). For reverse transcription, oligos with custom barcodes were used (Supplementary Table 1) and the cDNA was purified and PCR amplified. The resulting product was gel purified (Novex 10% TBE gel) and cleaned using ChIP DNA clean & Concentrator Kit (Zymo D5205).

ATAC-seq

ATAC-seq60 was performed in two biological replicates per condition from 5 × 10^4 nuclei per replicate using Nextera Tn5 Transposase (Illumina FC-121-1030, 30 min, 37º). DNA was purified by Qiagen MinElute Kit. Transposed fragments were amplified with NEBNext High-Fidelity PCR Master Mix (NEB M0541). Libraries were cleaned and size-selected using AMPure beads (Agilent) and assessed by Bioanalyzer and Qubit.

ChIP-seq and ChIP-qPCR

For H3 and H3K27Ac ChIP, cells were crosslinked with 1% formaldehyde, lysed and sonicated (Bioruptor, Diagenode) for 40 cycles and power H in 1% Triton, 0.1% Sodium Deoxycholate, 0.5% SDS, 0.2 M NaCl, 10 mM Tris pH 7.5, 10 mM EDTA. Lysates were incubated for 16 h with anti-H3 (Abcam ab1791) and anti-H3K27Ac (Abcam ab4729) pre-bound to protein G Dynabeads (Invitrogen 10004D) in RIPA buffer. Beads were washed and reverse-crosslinked by incubation at 65ºC, 10% SDS. DNA was purified using ChIP DNA clean & Concentrator Kit (Zymo D5205). For RAD21 ChIP cells were sonicated for 25 cycles at power H in 1% Triton, 0.1% Sodium Deoxycholate, 0.1% SDS, 0.8M NaCl, 10mM Tris pH 7.5, 1 mM EDTA, and incubated for 16 h with anti-RAD21 (Abcam ab992). Libraries were prepared using a NEBNext Ultra DNA LIbrary Prep kit (New England Biolabs E7370).

4C-seq

4C template preparation was performed as described3,61 with modifications. Briefly, macrophages were crosslinked in PBS with 1% formaldehyde at 20-25°C for 10 minutes and nuclei were isolated in lysis buffer (10 mM Tris-HCl pH 7.4, 150 mM NaCl, 0.5% NP-40, 5 mM EDTA, proteinase inhibitors). The first digestion was performed by using MboI, digestion products were ligated by T4 DNA ligase. Then, the 3C templates were digested by the second enzyme, NlaIII, and the digested DNA fragments were ligated again. 4C data analysis was performed using the 4Cseqpipe software suite62 and the setting values of nearcis were "-stat_type mean -trend_resolution 5000". PCR primers used are listed Supplementary table 1.

5C

3C templates were obtained crosslinking cells with 1% formaldehyde for 10 min at 20-25°C. 1×10^7 cells were lysed in 500 μl of lysis buffer (10 mM Tris-HCl pH8.0, 10 mM NaCl, 0.2% NP-40, 1 × protease inhibitor) for 15 min on ice and disrupted with 15 strokes of a p1000 pipette. After centrifugation, nuclei were resuspended in 500 μl digestion buffer and pierced adding SDS (0.1%, 10 min, 65°C). SDS was quenched with Triton-X100 (1%). DNA was digested with HindIII (800U, 37°C, 16 h). After inactivation by SDS (1.6%, 65°C, 20 min), samples were diluted in 7.5 ml 1× ligation buffer and 3000 NEB Units T4 ligase and incubated at 16°C for 4 h. Ligated chromatin was digested by proteinase K for 16 h. DNA was phenol-chloroform extracted and ethanol-precipitated. 3 fM of 5C primers were annealed to the junctions of the 3C material for 16 h at 48°C, joined with 10U of NAD-dependent ligase for 1 h, and amplified by 25 PCR cycles using T3 and T7 universal primers. Libraries were sequenced to 30×10^6 100bp paired-end reads on an Illumina Hi-seq 2000. Forward and reverse 5C primers were designed using my5C software (http://3dg.umassmed.edu/my5Cprimers/5C.php) to interrogate interactions between HindIII fragments containing transcription start sites (TSSs) and any other HindIII restriction fragments (distal fragments) in the ~5Mb interval (80,141,160-85,160,410 on mouse chr 11). Multiplex 5C libraries were produced by mixing 171 reverse primers annealing to the TSS of all genes in the region (ca. 3 restriction fragments per TSS), 581 forward primers annealing to all other restriction fragments and 21 reverse primers with 20 forward primers corresponding to random restriction fragments on a gene desert region (Chr 14) to assess 99,351 possible contacts.

RNA-Seq analysis

100bp paired end RNASeq reads were aligned to mouse genome mm9 using Tophat2 63 with arguments *"--library-type fr-firststrand --b2-very-sensitive --b2-L 25"* with gene annotation from Ensembl version 67. Read counts on genes were summarized using HTSeq-count64. Differentially expressed genes were identified using DESeq2 65. FPKM values were computed in R and heatmaps were drawn using rlog values for inducible genes23 using R package heatmap3.

Gene set enrichment analysis

GSEA was carried out using ranked gene list based on wald statistics from DESeq2 results using MSigDB gene sets66. Genes with low read counts were excluded from the analysis by using DESeq2 independent filtering approach. Gene ontology analysis was performed using the GOSeq R package67 and pathway analysis using Panther68.

ChIP-Seq analysis

ChIP-Seq and input libraries were sequenced and 50bp single end reads aligned to mouse genome mm9 using Bowtie version 0.12.8. Duplicate reads and reads aligning to >1 genomic positions were discarded. Quality was assessed using ChIPQC69. Genome wide coverage tracks were generated using ‘coverage’ function in ‘GenomicRanges’ R package, exported as bigwig, and visualized using UCSC genome browser. ChIP-Seq Peaks were identified by MACS270 using input libraries. RAD21 consensus peaks were derived by taking the intersection of RAD21 peaks identified in each biological replicate. Genes were marked as RAD21-bound if there was a RAD21 peak overlapping or within 10kb of the gene. Reads on enhancers22 were summarized using the summarizeOverlaps function of the GenomicAlignments R package. Enhancers with differential enrichment of H3K27Ac were identified by DESeq2.

GRO-Seq analysis

GRO-Seq libraries were sequenced as 50 bp single end reads in 2 biological replicates. The 10 most 3’ bases were discarded based on fastqc quality assessment. Reads were aligned to mouse genome mm9 using bowtie with arguments '-l 30 -m 10 -n 2 – trim3 10'. Read counts on enhancers were computed using summarizeOverlaps function from GeomicAlignments R Package. Differentially transcribed enhancers were identified using DESeq2.

Motif enrichment analysis

Enrichment of known transcription factor motifs in enhancer TSS was performed using Homer’s findMotifsGenome.pl program with default parameters71. The analysis was restricted to intergenic enhancer TSS identified from GRO-seq signal46 that were extended ± 100 bp. If an enhancer had multiple TSS, all were included in the analysis. Strongly inducible enhancers were classified by DESeq2 analysis of H3K27ac in wild-type macrophages 1 or 6 h after LPS stimulation compared to unstimulated cells ($\log_2$ FC > 1.5 and Benjamini and Hochberg-adjusted $P < 0.05$). Failed enhancers were identified by comparing H3K27ac in *Rad21*-deleted macrophages with wild-type macrophages at each time point ($\log_2$ FC = 0 and Benjamini and Hochberg-adjusted $P < 0.05$). Maintained enhancers were used as background for failed enhancer motif enrichment analysis and *vice versa*. Motif occurrences in enhancers were identified using Homer’s findMotifsGenome.pl program.

Enhancer analysis

Unless otherwise indicated, the analysis of enhancers was based on22. Of 8991 constitutive enhancers ('constitutive steady'22), 3775 were intergenic, and 7082, 6984, and 8188 were included in DESeq2 at 0, 1 and 6 h. Of 6708 inducible enhancers (union of 'constitutive not

steady', 'poised activated' and 'cryptic' 22), 2893 were intergenic, and 3713, 4106, and 5903 were included in DESeq2 at 0, 1 and 6 h. Of 11146 LPS-repressed enhancers22, 4914 were intergenic, and 8787, 7969, and 9786 were included in DESeq2 at 0, 1 and 6 h. DESeq2 was used to identify enhancer deregulation within the three groups at each time point based on H3K27ac, GRO-seq or ATAC-seq (Benjamini and Hochberg-adjusted $P < 0.05$). FPKM values for H3K27ac, Rad21, H3 and GRO-seq datasets on enhancers were generated in R. Heatmaps were generated using the heatmap3 R package. Super-enhancers were defined using ROSE72. Peaks identified using H3K27ac ChIP-seq were used as input to ROSE. Promoters (TSS ± 2.5 kb) were excluded from the analysis.

ATAC-Seq analysis

ATAC-Seq libraries were sequenced as 100 bp paired end in 2 biological replicates. FastQC and found that bases 35-100 were enriched for “Nextera transposase adapter” sequences. Therefore, reads were aligned to Mouse genome mm9 using bowtie v0.12.8 with arguments *“--chunkmbs 256 -S -n 2 -m 1 -p 8 -X 2000”* by successively trimming 10bases from 3’ end down to a read length of 40bp. Uniquely aligned reads were retained. Duplicate reads were identified using Picard MarkDuplicates. Aligned reads in Watson strand were offset by +4 bp and reads aligned to Crick strand were offset by -5 bp as described60. Reads from fragments < 120bp were considered unprotected. Accessibility peaks for each replicate were identified using MACS270 with arguments “--nomodel –nolambda”. We defined consensus accessibility peaks by taking the intersection of peaks from both biological replicates. Read counts on enhancers and accessibility peaks were computed using summarizeOverlaps and differentially accessible regions were identified by DESeq2. Aaccessibility plots were generated using SoGGi R Package with reads counts normalized to sequencing depth.

TCGA RNA-seq analysis

TCGA RNA-seq analysis. TCGA IlluminaHiSeq_RNASeqV2 dataset was obtained for 173 AML patients via the GDC Legacy Archive (https://portal.gdc.cancer.gov/legacy-archive/search/f). Raw gene counts for each patient were converted to counts per million (CPM) using the function *cpm* from the R/Bioconductor package *edgeR* (3.16.5)73,74. Lowly expressed genes were removed if CPM was < 1. Normalisation was performed by trimmed mean of M-values (TMM)75 using the *calcNormFactors* function in *edgeR*. R/Bioconductor package *limma*(3.30.12)76 was applied for the differential expression analysis, and the function *voom*77 was used to transfer raw counts to $\log_2$-counts per million (logCPM). Differential expression analysis between AMLs was performed by the *lmFit* and *eBayes*78 functions in *limma*. Genes were ranked by moderated T-statistics and gene set enrichment analysis (GSEA)66 was applied using hallmark gene sets from MSigDB79. Oncoprint, mutations and clinical information were obtained from cBioportal80.

5C analysis

After quality filtering, 101 nt paired-end reads were trimmed (4 bases at the 5’ and 50 bases at the 3’) using the fastx_trimmer tool (FASTX-Toolkit, http://hannonlab.cshl.edu/fastx_toolkit/). Trimmed reads were aligned to the primer pool using Novoalign (http://novocraft.com, version 3). Considering all possible forward-reverse pairs, interactions were summarized as a matrix. 5C data was analysed at fragment level using HiTC (v1.18.1)81 and

normalized using the square root of the coverage of each fragment3. Enhancer-promoter interactions were defined as interactions between a fragment overlapping an enhancer22 and a fragment overlapping an annotated promoter (Ensembl v67) using the linkOverlaps function from the InteractionSet package v1.2.1 with default parameters82. Data was visualized using GenomicInteractions v1.7.1 and Gviz (v1.18.2)83,84. The normalized strength of the given set of interactions (e.g. interactions involving inducible promoters) was compared at each time point to the normalized strength of all other enhancer-promoter interactions using a Wilcoxon rank sum test. *P*-values were corrected for multiple testing using the p.adjust function in R, and adjusted $P < 0.05$ was considered significant.

TAD analysis

CH12 TADs were defined using Tadtool85 on pre-processed Hi-C matrices3 using the "ninsulation" algorithm with a window size of 400 kb and a cutoff of 0.15. To identify TADs enriched for classes of genes/enhancers, a binomial test approach was used. First, genes and enhancers were assigned to TADs using the findOverlaps function from the GenomicRanges package in R. Promoter regions were defined as 100bp regions around annotated transcription start sites (Ensembl v67) and used to assign genes to TADs. Enhancers were assigned to TADs based on published enhancer coordinates (31), < 1% of enhancers and promoters are assigned to > 1 TAD.

For each class of enhancer and for each TAD, the number of enhancers of that class (e.g. enhancers with downregulated H2K27ac), given the number of total enhancers in the TAD, was compared to the fraction of all enhancers in that class, using the binom.test function in R with alternative = "greater". The resulting *P*-values were corrected for multiple testing using the p.adjust function in R with method "BH" and domains were considered significantly enriched for a class of enhancers at adj. $P < 0.05$. The same analysis was performed for genes.

Definition of IFN-dependent genes

IFN-dependent inducible genes included STAT target genes86 and antiviral response genes87 as curated previously24.

Statistics and reproducibility

Statistical analysis were calculated with GraphPad Prism version 7 (two-tailed Student's *t* tests) or R version 3.2.3 (Fisher exact tests) as indicated in the figure legends. Statistical differences were considered significant when $P \leq 0.05$. Error bars are reported as SEM. Experiments were repeated independently at least three times.

Supplementary Material

Refer to Web version on PubMed Central for supplementary material.

Acknowledgements

We thank A. Innes, M. Spivakov and D. Odom (CRUK Cambridge) for discussion, L Game for sequencing, J Elliott and the LMS/NIHR Imperial Biomedical Research Centre Flow Cytometry Facility for cell sorting. This work was

funded by Wellcome Investigator Award 099276/Z/12/Z (M.M.), Wellcome Project Grant P55504 (B.L.), Fundação de Amparo à Pesquisa do Estado de São Paulo 2014/20861-3 (M.T.A.), Academy of Finland grants #287478 and #294073 (M.U.K), MRC Programme Grant ID 84637 and Wellcome Trust Programme Grant Ref 078241/Z/05/Z (K.A.M.), ERC grant #692789 (G.N.), and core support from the Medical Research Council UK to the London Institute of Medical Sciences.

References

1. Fudenberg G, et al. Formation of Chromosomal Domains by Loop Extrusion. Cell Rep. 2016; 15:2038–49. [PubMed: 27210764]
2. Nora EP, et al. Targeted Degradation of CTCF Decouples Local Insulation of Chromosome Domains from Genomic Compartmentalization. Cell. 2017; 169:930–944. [PubMed: 28525758]
3. Rao SSP, et al. A 3D map of the human genome at kilobase resolution reveals principles of chromatin looping. Cell. 2014; 159:1665–1680. [PubMed: 25497547]
4. Rao SSP, et al. Cohesin Loss Eliminates All Loop Domains. Cell. 2017; 171:305–320. [PubMed: 28985562]
5. Dowen JM, et al. Control of Cell Identity Genes Occurs in Insulated Neighborhoods in Mammalian Chromosomes. Cell. 2014; 159:374–387. [PubMed: 25303531]
6. Hnisz D, Day DS, Young RA. Insulated Neighborhoods: Structural and Functional Units of Mammalian Gene Control. Cell. 2016; 167:1188–1200. [PubMed: 27863240]
7. Schwarzer W, et al. Two independent modes of chromatin organization revealed by cohesin removal. Nature. 2017; 551:51. [PubMed: 29094699]
8. Merkenschlager M, Nora EP. CTCF and Cohesin in Genome Folding and Transcriptional Gene Regulation. Annu Rev Genomics Hum Genet. 2016; 17:17–43. [PubMed: 27089971]
9. Dekker J, Heard E. Structural and functional diversity of Topologically Associating Domains. FEBS Lett. 2015; 589:2877–2884. [PubMed: 26348399]
10. Dekker J, Mirny L. The 3D Genome as Moderator of Chromosomal Communication. Cell. 2016; 164:1110–1121. [PubMed: 26967279]
11. Bickmore WA, van Steensel B. Genome Architecture: Domain Organization of Interphase Chromosomes. Cell. 2013; 152:1270–1284. [PubMed: 23498936]
12. Hnisz D, et al. Activation of proto-oncogenes by disruption of chromosome neighborhoods. Science. 2016; 351:1454–1458. [PubMed: 26940867]
13. Jiang Y, et al. The methyltransferase SETDB1 regulates a large neuron-specific topological chromatin domain. Nat Genet. 2017; 49:1239–1250. [PubMed: 28671686]
14. Mansour MR, et al. An oncogenic super-enhancer formed through somatic mutation of a noncoding intergenic element. Science. 2014; 346:1373–1377. [PubMed: 25394790]
15. Lupiáñez DG, et al. Disruptions of Topological Chromatin Domains Cause Pathogenic Rewiring of Gene-Enhancer Interactions. Cell. 2015; 161:1012–1025. [PubMed: 25959774]
16. Narendra V, et al. CTCF establishes discrete functional chromatin domains at the Hox clusters during differentiation. Science. 2015; 347:1017–1021. [PubMed: 25722416]
17. Seitan VC, et al. A role for cohesin in T-cell-receptor rearrangement and thymocyte differentiation. Nature. 2011; 476:467–471. [PubMed: 21832993]
18. Kagey MH, et al. Mediator and cohesin connect gene expression and chromatin architecture. Nature. 2010; 467:430–435. [PubMed: 20720539]
19. Lavagnolli T, et al. Initiation and maintenance of pluripotency gene expression in the absence of cohesin. Genes Dev. 2015; 29:23–38. [PubMed: 25561493]
20. Ing-Simmons E, et al. Spatial enhancer clustering and regulation of enhancer-proximal genes by cohesin. Genome Res. 2015; 25:504–513. [PubMed: 25677180]
21. Kaikkonen MU, et al. Remodeling of the Enhancer Landscape during Macrophage Activation Is Coupled to Enhancer Transcription. Mol Cell. 2013; 51:310–325. [PubMed: 23932714]
22. Ostuni R, et al. Latent Enhancers Activated by Stimulation in Differentiated Cells. Cell. 2013; 152:157–171. [PubMed: 23332752]
23. Bhatt DM, et al. Transcript Dynamics of Proinflammatory Genes Revealed by Sequence Analysis of Subcellular RNA Fractions. Cell. 2012; 150:279–290. [PubMed: 22817891]

24. Chen X, et al. Requirement for the histone deacetylase Hdac3 for the inflammatory gene expression program in macrophages. Proc Natl Acad Sci. 2012; 109:E2865–E2874. [PubMed: 22802645]
25. Glass CK, Natoli G. Molecular control of activation and priming in macrophages. Nat Immunol. 2016; 17:26–33. [PubMed: 26681459]
26. Nasmyth K, Haering CH. Cohesin: Its Roles and Mechanisms. Annu Rev Genet. 2009; 43:525–558. [PubMed: 19886810]
27. Kon A, et al. Recurrent mutations in multiple components of the cohesin complex in myeloid neoplasms. Nat Genet. 2013; 45:1232–1237. [PubMed: 23955599]
28. Cancer Genome Atlas Research Network. Genomic and Epigenomic Landscapes of Adult De Novo Acute Myeloid Leukemia. N Engl J Med. 2013; 368:2059–2074. [PubMed: 23634996]
29. Thota S, et al. Genetic alterations of the cohesin complex genes in myeloid malignancies. Blood. 2014; 124:1790–1798. [PubMed: 25006131]
30. Mazumdar C, et al. Leukemia-Associated Cohesin Mutants Dominantly Enforce Stem Cell Programs and Impair Human Hematopoietic Progenitor Differentiation. Cell Stem Cell. 2015; 17:675–688. [PubMed: 26607380]
31. Mullenders J, et al. Cohesin loss alters adult hematopoietic stem cell homeostasis, leading to myeloproliferative neoplasms. J Exp Med. 2015; 212:1833–1850. [PubMed: 26438359]
32. Viny AD, et al. Dose-dependent role of the cohesin complex in normal and malignant hematopoiesis. J Exp Med. 2015; 212:1819–1832. [PubMed: 26438361]
33. Galeev R, et al. Genome-wide RNAi Screen Identifies Cohesin Genes as Modifiers of Renewal and Differentiation in Human HSCs. Cell Rep. 2016; 14:2988–3000. [PubMed: 26997282]
34. Fisher JB, et al. The cohesin subunit Rad21 is a negative regulator of hematopoietic self-renewal through epigenetic repression of Hoxa7 and Hoxa9. Leukemia. 2017; 31:712–719. [PubMed: 27554164]
35. Baldridge MT, King KY, Boles NC, Weksberg DC, Goodell MA. Quiescent haematopoietic stem cells are activated by IFN-γ in response to chronic infection. Nature. 2010; 465:793–797. [PubMed: 20535209]
36. Binder D, et al. Aplastic anemia rescued by exhaustion of cytokine-secreting CD8+ T cells in persistent infection with lymphocytic choriomeningitis virus. J Exp Med. 1998; 187:1903–20. [PubMed: 9607930]
37. Dybedal I, Bryder D, Fossum A, Rusten LS, Jacobsen SE. Tumor necrosis factor (TNF)-mediated activation of the p55 TNF receptor negatively regulates maintenance of cycling reconstituting human hematopoietic stem cells. Blood. 2001; 98:1782–91. [PubMed: 11535512]
38. Essers MAG, et al. IFNα activates dormant haematopoietic stem cells in vivo. Nature. 2009; 458:904–908. [PubMed: 19212321]
39. Mossadegh-Keller N, et al. M-CSF instructs myeloid lineage fate in single haematopoietic stem cells. Nature. 2013; 497:239–243. [PubMed: 23575636]
40. Nagai Y, et al. Toll-like Receptors on Hematopoietic Progenitor Cells Stimulate Innate Immune System Replenishment. Immunity. 2006; 24:801–812. [PubMed: 16782035]
41. Pietras EM, et al. Chronic interleukin-1 exposure drives haematopoietic stem cells towards precocious myeloid differentiation at the expense of self-renewal. Nat Cell Biol. 2016; 18:607–618. [PubMed: 27111842]
42. Zhao JL, et al. Conversion of Danger Signals into Cytokine Signals by Hematopoietic Stem and Progenitor Cells for Regulation of Stress-Induced Hematopoiesis. Cell Stem Cell. 2014; 14:445–459. [PubMed: 24561084]
43. Bennett JM, et al. Proposals for the classification of the acute leukaemias. French-American-British (FAB) co-operative group. Br J Haematol. 1976; 33:451–8. [PubMed: 188440]
44. Tachibana-Konwalski K, et al. Rec8-containing cohesin maintains bivalents without turnover during the growing phase of mouse oocytes. Genes Dev. 2010; 24:2505–2516. [PubMed: 20971813]
45. Zlotnik A, Yoshie O, Nomiyama H. The chemokine and chemokine receptor superfamilies and their molecular evolution. Genome Biol. 2006; 7:243. [PubMed: 17201934]

46. Azofeifa JG, Allen MA, Lladser ME, Dowell RD. An Annotation Agnostic Algorithm for Detecting Nascent RNA Transcripts in GRO-Seq. IEEE/ACM Trans Comput Biol Bioinformatics. 2017; 14:1070–1081.
47. Hakimi M-A, et al. A chromatin remodelling complex that loads cohesin onto human chromosomes. Nature. 2002; 418:994–998. [PubMed: 12198550]
48. Faure AJ, et al. Cohesin regulates tissue-specific expression by stabilizing highly occupied cis-regulatory modules. Genome Res. 2012; 22:2163–2175. [PubMed: 22780989]
49. Yan J, et al. Transcription Factor Binding in Human Cells Occurs in Dense Clusters Formed around Cohesin Anchor Sites. Cell. 2013; 154:801–813. [PubMed: 23953112]
50. Lopez-Serra L, Kelly G, Patel H, Stewart A, Uhlmann F. The Scc2–Scc4 complex acts in sister chromatid cohesion and transcriptional regulation by maintaining nucleosome-free regions. Nat Genet. 2014; 46:1147–1151. [PubMed: 25173104]
51. Schieber TA, et al. Information theory perspective on network robustness. Phys Lett A. 2016; 380:359–364.
52. Painter MW, Davis S, Hardy RR, Mathis D, Benoist C. Transcriptomes of the B and T Lineages Compared by Multiplatform Microarray Profiling. J Immunol. 2011; 186:3047–3057. [PubMed: 21307297]
53. Matatall KA, et al. Chronic Infection Depletes Hematopoietic Stem Cells through Stress-Induced Terminal Differentiation. Cell Rep. 2016; 17:2584–2595. [PubMed: 27926863]
54. Shalek AK, et al. Single-cell RNA-seq reveals dynamic paracrine control of cellular variation. Nature. 2014; 510:363–369. [PubMed: 24919153]
55. Heidinger-Pauli JM, Mert O, Davenport C, Guacci V, Koshland D. Systematic Reduction of Cohesin Differentially Affects Chromosome Segregation, Condensation, and DNA Repair. Curr Biol. 2010; 20:957–963. [PubMed: 20451387]
56. Deardorff MA, Noon SE, Krantz ID. Cornelia de Lange Syndrome. GeneReviews®. Seattle (WA): University of Washington, Seattle; 1993-2018; 2005. Sep 16, [Internet] [updated 2016 Jan 28]
57. Seibler J, et al. Rapid generation of inducible mouse mutants. Nucleic Acids Res. 2003; 31:e12. [PubMed: 12582257]
58. Cobb BS, et al. Targeting of Ikaros to pericentromeric heterochromatin by direct DNA binding. Genes Dev. 2000; 14:2146–60. [PubMed: 10970879]
59. Carpenter AE, et al. CellProfiler: image analysis software for identifying and quantifying cell phenotypes. Genome Biol. 2006; 7:R100. [PubMed: 17076895]
60. Buenrostro JD, Giresi PG, Zaba LC, Chang HY, Greenleaf WJ. Transposition of native chromatin for fast and sensitive epigenomic profiling of open chromatin, DNA-binding proteins and nucleosome position. Nat Methods. 2013; 10:1213–1218. [PubMed: 24097267]
61. Splinter E, de Wit E, van de Werken HJG, Klous P, de Laat W. Determining long-range chromatin interactions for selected genomic sites using 4C-seq technology: From fixation to computation. Methods. 2012; 58:221–230. [PubMed: 22609568]
62. van de Werken HJG, et al. Robust 4C-seq data analysis to screen for regulatory DNA interactions. Nat Methods. 2012; 9:969–972. [PubMed: 22961246]
63. Kim D, et al. TopHat2: accurate alignment of transcriptomes in the presence of insertions, deletions and gene fusions. Genome Biol. 2013; 14:R36. [PubMed: 23618408]
64. Anders S, Pyl PT, Huber W. HTSeq--a Python framework to work with high-throughput sequencing data. Bioinformatics. 2015; 31:166–9. [PubMed: 25260700]
65. Love MI, Huber W, Anders S. Moderated estimation of fold change and dispersion for RNA-seq data with DESeq2. Genome Biol. 2014; 15:550. [PubMed: 25516281]
66. Subramanian A, et al. Gene set enrichment analysis: a knowledge-based approach for interpreting genome-wide expression profiles. Proc Natl Acad Sci U S A. 2005; 102:15545–50. [PubMed: 16199517]
67. Young MD, Wakefield MJ, Smyth GK, Oshlack A. Gene ontology analysis for RNA-seq: accounting for selection bias. Genome Biol. 2010; 11:R14. [PubMed: 20132535]

68. Mi H, et al. PANTHER version 11: expanded annotation data from Gene Ontology and Reactome pathways, and data analysis tool enhancements. Nucleic Acids Res. 2017; 45:D183–D189. [PubMed: 27899595]
69. Carroll TS, Liang Z, Salama R, Stark R, de Santiago I. Impact of artifact removal on ChIP quality metrics in ChIP-seq and ChIP-exo data. Front Genet. 2014; 5:75. [PubMed: 24782889]
70. Zhang Y, et al. Model-based Analysis of ChIP-Seq (MACS). Genome Biol. 2008; 9:R137. [PubMed: 18798982]
71. Heinz S, et al. Simple Combinations of Lineage-Determining Transcription Factors Prime cis-Regulatory Elements Required for Macrophage and B Cell Identities. Mol Cell. 2010; 38:576–589. [PubMed: 20513432]
72. Whyte WA, et al. Master Transcription Factors and Mediator Establish Super-Enhancers at Key Cell Identity Genes. Cell. 2013; 153:307–319. [PubMed: 23582322]
73. Robinson MD, McCarthy DJ, Smyth GK. edgeR: a Bioconductor package for differential expression analysis of digital gene expression data. Bioinformatics. 2010; 26:139–140. [PubMed: 19910308]
74. McCarthy DJ, Chen Y, Smyth GK. Differential expression analysis of multifactor RNA-Seq experiments with respect to biological variation. Nucleic Acids Res. 2012; 40:4288–97. [PubMed: 22287627]
75. Robinson MD, Oshlack A. A scaling normalization method for differential expression analysis of RNA-seq data. Genome Biol. 2010; 11:R25. [PubMed: 20196867]
76. Ritchie ME, et al. limma powers differential expression analyses for RNA-sequencing and microarray studies. Nucleic Acids Res. 2015; 43:e47–e47. [PubMed: 25605792]
77. Law CW, Chen Y, Shi W, Smyth GK. voom: precision weights unlock linear model analysis tools for RNA-seq read counts. Genome Biol. 2014; 15:R29. [PubMed: 24485249]
78. Phipson B, Lee S, Majewski IJ, Alexander WS, Smyth GK. Robust hyperparameter estimation protects against hypervariable genes and improves power to detect differential expression. Ann Appl Stat. 2016; 10:946–963. [PubMed: 28367255]
79. Liberzon A, et al. The Molecular Signatures Database Hallmark Gene Set Collection. Cell Syst. 2015; 1:417–425. [PubMed: 26771021]
80. Cerami E, et al. The cBio Cancer Genomics Portal: An Open Platform for Exploring Multidimensional Cancer Genomics Data: Figure 1. Cancer Discov. 2012; 2:401–404. [PubMed: 22588877]
81. Servant N, et al. HiTC: exploration of high-throughput ‘C’ experiments. Bioinformatics. 2012; 28:2843–2844. [PubMed: 22923296]
82. Lun ATL, Perry M, Ing-Simmons E. Infrastructure for genomic interactions: Bioconductor classes for Hi-C, ChIA-PET and related experiments. F1000Research. 2016; 5:950. [PubMed: 27303634]
83. Harmston N, Ing-Simmons E, Perry M, Barešić A, Lenhard B. GenomicInteractions: An R/Bioconductor package for manipulating and investigating chromatin interaction data. BMC Genomics. 2015; 16:963. [PubMed: 26576536]
84. Hahne F, Ivanek R. Visualizing Genomic Data Using Gviz and Bioconductor. Methods in molecular biology (Clifton, N. J.). 2016; 1418:335–351.
85. Kruse K, Hug CB, Hernández-Rodríguez B, Vaquerizas JM. TADtool: visual parameter identification for TAD-calling algorithms. Bioinformatics. 2016; 32:3190–3192. [PubMed: 27318199]
86. Amit I, et al. Unbiased Reconstruction of a Mammalian Transcriptional Network Mediating Pathogen Responses. Science. 2009; 326:257–263. [PubMed: 19729616]
87. Garber M, et al. A High-Throughput Chromatin Immunoprecipitation Approach Reveals Principles of Dynamic Gene Regulation in Mammals. Mol Cell. 2012; 47:810–822. [PubMed: 22940246]

Europe PMC Funders Author Manuscripts

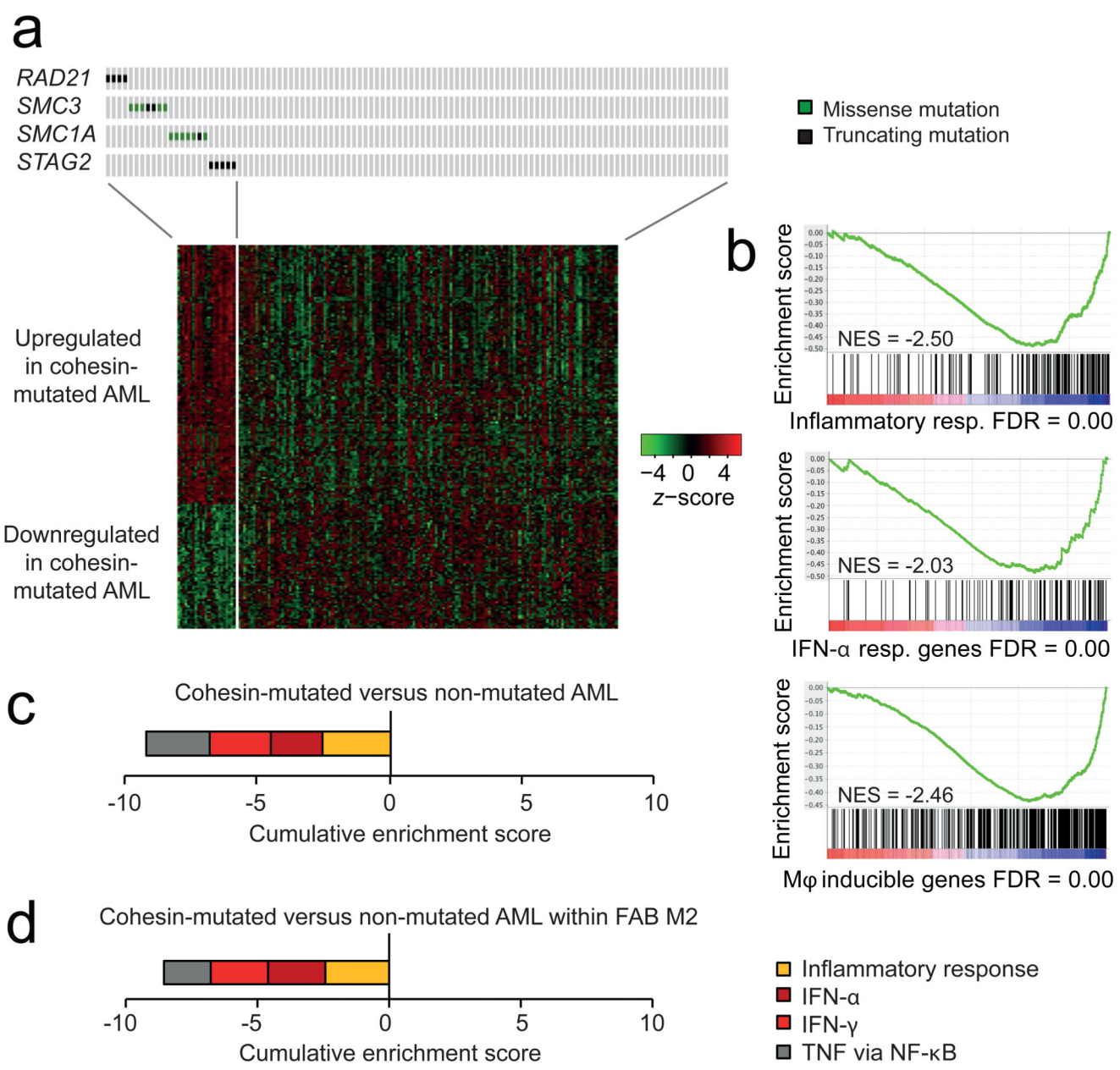

Figure 1. Cohesin links inflammation and cancer

a) Analysis of RNA-seq data from 173 primary human TCGA AML, 23 of which had missense or truncating mutations in the cohesin genes *RAD21, SMC3, SMC1A* or *STAG2* showed significant upregulation of 131 genes and downregulation of 63 genes in cohesin-mutated AML compared to 150 AML without cohesin mutations, (adj. $P < 0.05$). Differential expression was analyzed and *z*-scores were calculated from normalized expression values as detailed in Methods.

b) GSEA of 23 TCGA AML with and 150 TCGA AML without cohesin mutations. Top, 'inflammatory response' genes (NES = -2.5, FDR = 0, see Methods), middle, IFN-α

response (NES = -2.03, FDR = 0), and bottom, the human orthologs of inducible mouse macrophage (Mϕ) genes23 in AML with cohesin mutations (NES = -2.46, FDR = 0).
c) Cumulative normalized enrichment score (NES) of significantly enriched or depleted gene sets for the pathways inflammatory response, IFN-α, IFN-γ, and TNF signaling via NF-κB (FDR < 0.05) in 23 TCGA AML with cohesin mutations compared to 150 TCGA AML without cohesin mutations.
d) Cumulative normalized enrichment score (NES) of significantly enriched or depleted gene sets for the pathways inflammatory response, IFN-α, IFN-γ, and TNF signaling via NF-κB (FDR < 0.05) in TCGA AML of FAB subtype M2, comparing 10 FAB subtype M2 AML with cohesin mutations and 27 FAB subtype M2 AML without cohesin mutations.

Europe PMC Funders Author Manuscripts

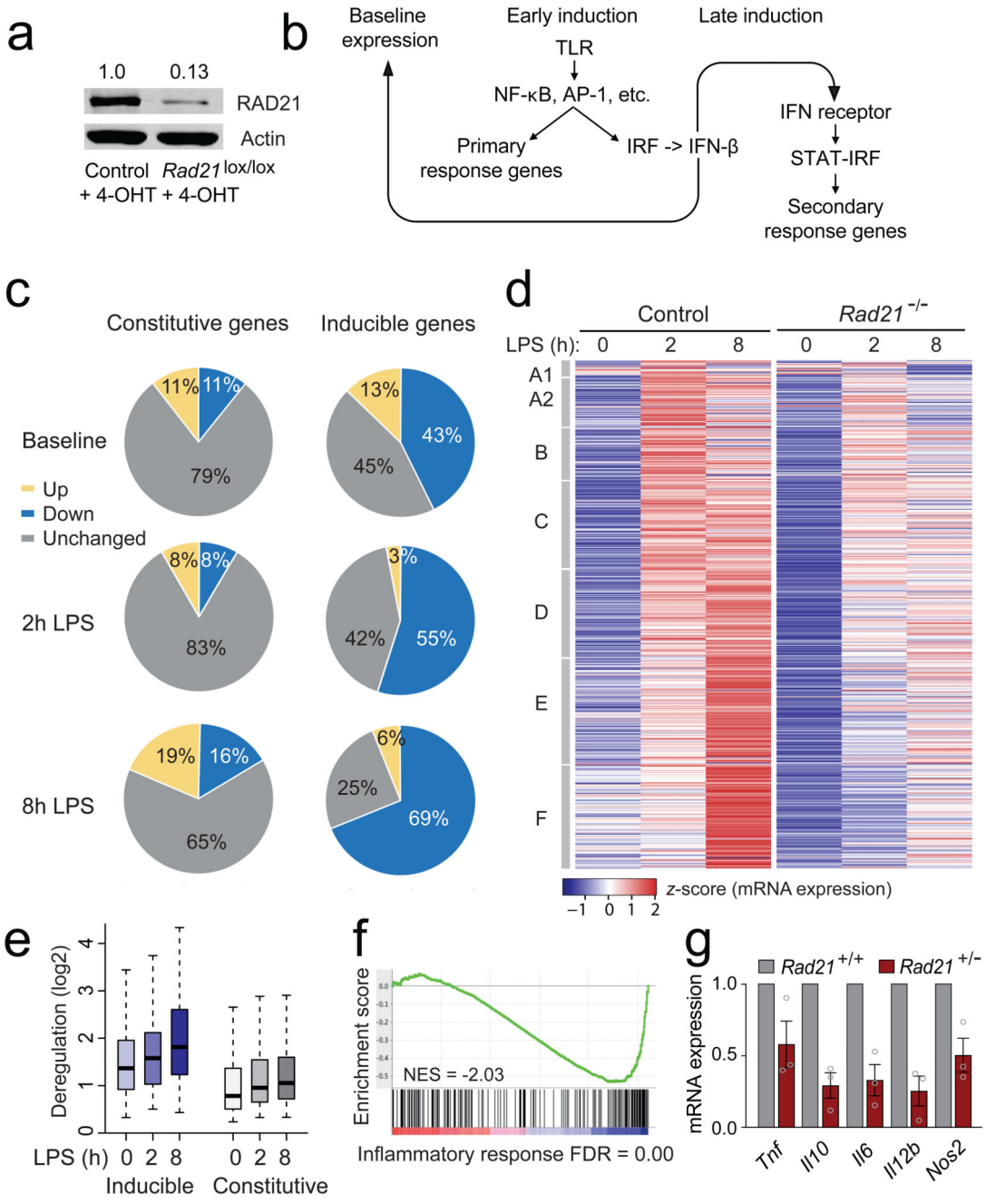

Figure 2. Cohesin promotes inducible gene expression

a) Immunoblot analysis of RAD21 protein expression in mature macrophages after *Rad21* deletion (mean 13.6% of control, 13 biological replicates).

b) Regulation of inducible genes at baseline and in response to macrophage activation21–25.

c) DEseq2 analysis of RNA-seq data was used to determine the fraction of constitutively expressed (n = 10,780) and LPS-inducible23 (n = 560) genes deregulated in *Rad21*$^{-/-}$ macrophages at baseline, and after 2 or 8 h of LPS stimulation (P < 0.05, 3 biological replicates per genotype and time point).

d) Heatmap of inducible gene expression by control (left) and *Rad21*-deleted macrophages (right) at 0, 2 and 8 h after LPS. Inducible gene classes23 are indicated on the left. Average of 3 biological replicates.

e) Extent of deregulation of inducible23 versus constitutive genes in *Rad21*-deleted compared to wild-type macrophages at baseline and after LPS (log_2, irrespective of direction). Box plots are representative of 3 biological RNA-seq replicates per genotype and condition and show the median and lower and upper quartiles. Whiskers show the maximum and minimum data points up to 1.5 times the interquartile range.

f) Gene set enrichment analysis of inflammatory response genes in *Rad21*-deleted macrophages (NES = -2.03, FDR = 0).

g) Quantitative RT-PCR of inflammatory gene expression 8 h after LPS stimulation of $Rad21^{+/-}$ macrophages (mean ± SEM of 3 biological replicates).

Europe PMC Funders Author Manuscripts

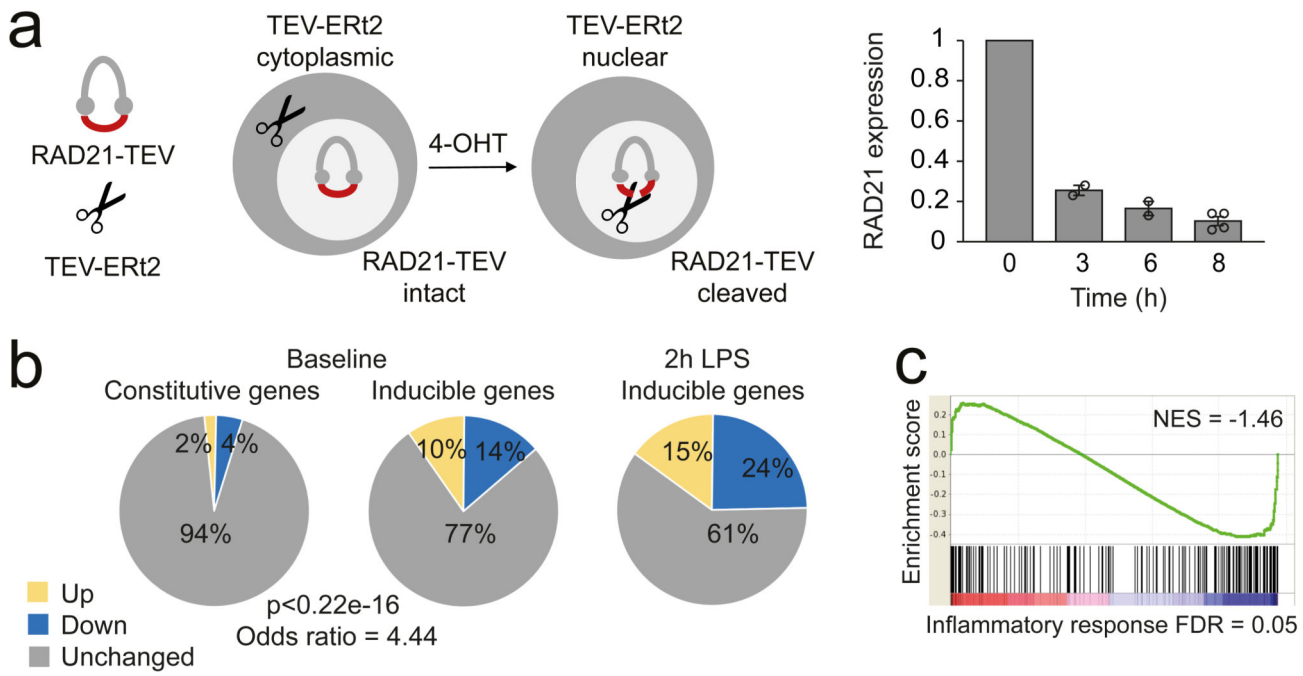

Figure 3. Identification of immediate cohesin target genes

a) Experimental system for TEV-induced cleavage of RAD21-TEV. Macrophages were generated from the livers of *Rad21*-TEV-Myc embryos44. RAD21 protein was quantified by fluorescent immunoblotting for the Myc tag and normalized to Actin (mean ± SEM of 2-4 biological replicates per time point).

b) Changes in constitutive and inducible23 gene expression in response to RAD21-TEV cleavage (4-OHT versus carrier) identified by DEseq2 analysis of RNA-seq data ($P < 0.05$, 3 biological replicates per genotype and time point). *P*-value and odds ratio were determined by two-sided Fisher's exact test between constitutive and inducible genes at baseline. Inducible genes23 deregulated immediately after RAD21-TEV cleavage included 33 IFN-dependent24 (14 up-, 19 downregulated) and 86 IFN-independent genes24 (36 up-, 50 downregulated).

c) GSEA of inflammatory response genes at baseline (NES = -1.46, FDR = 0.05).

Europe PMC Funders Author Manuscripts

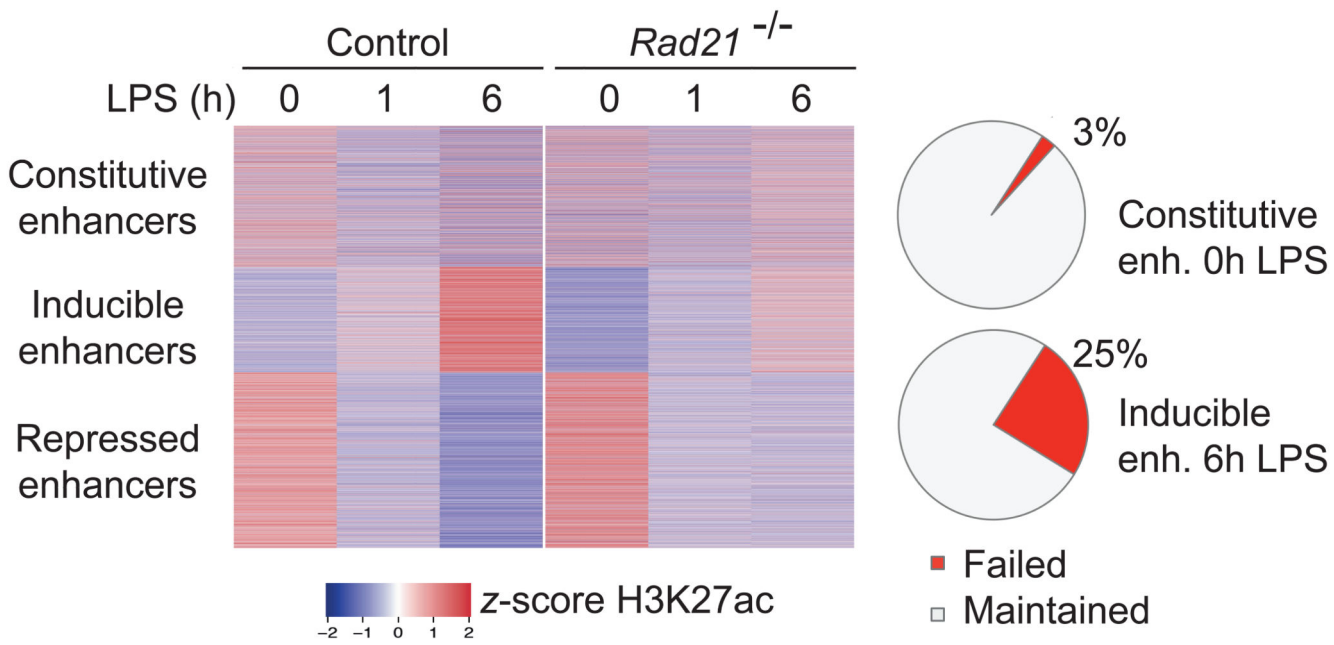

Figure 4. Restricted enhancer dynamics in cohesin-deficient macrophages

Left, Heatmap of H3K27ac ChIP-seq signals for constitutively active (8991), inducible (6708), and repressed (11146) enhancers22. *z*-scores were calculated based on FPKM. Right, Frequency of enhancers with deregulated H3K27ac in *Rad21*-deleted macrophages as determined by DESeq2 analysis of 2 H3K27ac ChIP-seq replicates (adj. $P < 0.05$).

Europe PMC Funders Author Manuscripts

Europe PMC Funders Author Manuscripts

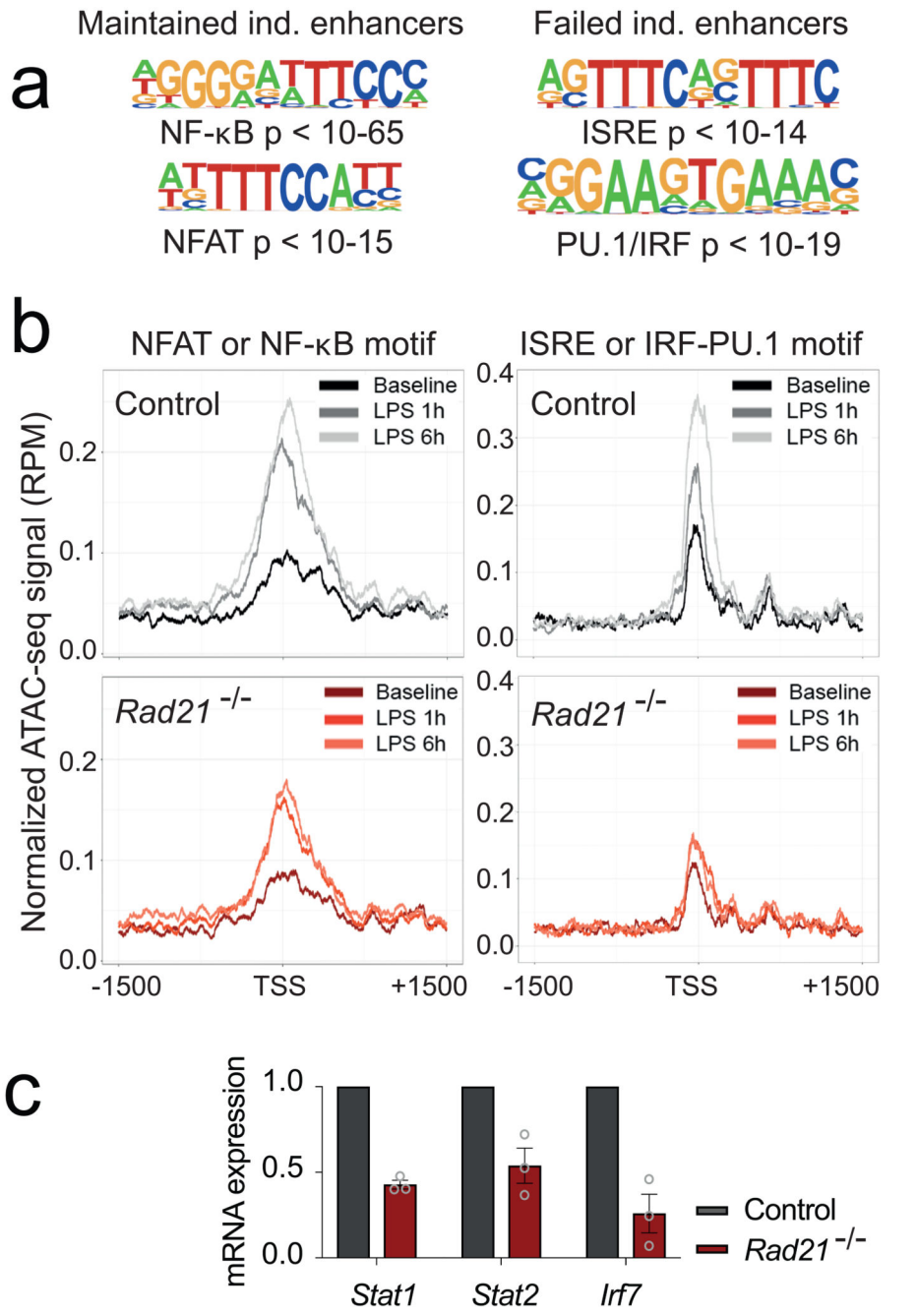

Figure 5. Inducible enhancers with ISRE or IRF-PU.1 motifs are more likely to fail

a) Inducible enhancers22 (H3K27ac $\log_2$ FC ≥ 1.5) with GRO-seq-mappable TSS were classified as failed (reduced H3K27ac in *Rad21*$^{-/-}$ macrophages, adj. $P < 0.05$) or maintained, and compared for enrichment of TSS-proximal transcription factor motifs. The 10 most highly enriched motifs were NF-κB (3 occurrences), NFAT (1), bHLH (2) Nuclear Receptors (2), Jun-CRE (1) and Fosl2 (1) at maintained inducible enhancers, and IRF and IFN-stimulated response element (ISRE, 5 occurrences), PU.1-IRF (2), KLF (2), and STAT (1) at failed inducible enhancers.

b) ATAC-seq accessibility of inducible enhancers with NFAT or NF-κB (top) versus ISRE or IRF-PU.1 motifs (bottom) in control (left) versus *Rad21*$^{-/-}$ macrophages (right).
c) Differential expression of *Stat1, Stat2* and *Irf7* in *Rad21*$^{-/-}$ macrophages relative to wild-type confirmed by quantitative RT-PCR. Mean ± SEM of 3 biological replicates, $P < 0.05$ by two-sided *t*-test.

Europe PMC Funders Author Manuscripts

Europe PMC Funders Author Manuscripts

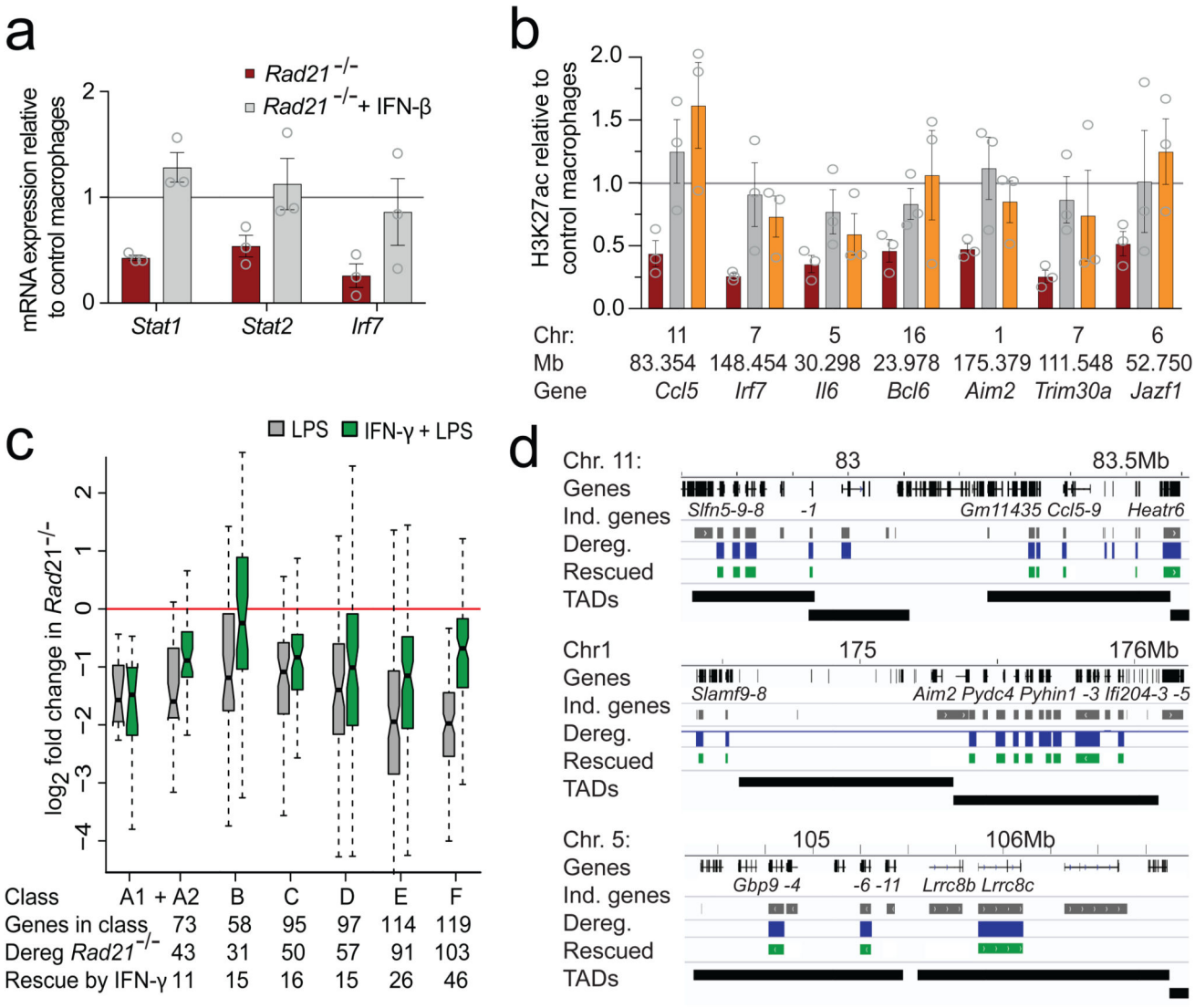

Figure 6. Rescue of inducible genes and enhancers in the absence of cohesin.

a) Quantitative RT-PCR analysis of *Stat1, Stat2* and *Irf7* expression by control and *Rad21*$^{-/-}$ macrophages. Expression in *Rad21*$^{-/-}$ relative to control macrophages with (grey) and without (red) IFN-β treatment for 24 h. Mean ± SEM of 3 biological replicates.

b) ChIP qPCR of histone H3-normalized H3K27ac in *Rad21*$^{-/-}$ relative to control macrophages at candidate inducible enhancers. The genomic coordinates and the nearest inducible gene are shown for each enhancer. Cells were cultured in medium (red), 10ng/ml IFN-γ (orange), or 100 U/ml IFN-β (grey) for 24 h prior to LPS-stimulation for 6 h. Mean ± SEM of 3 biological replicates.

c) Fold-change of early (2 h LPS, class A-D) and late (8 h LPS, class E, F) inducible genes23 in *Rad21*-/- over control macrophages with (green) or without (grey) 24 h IFN-γ pre-treatment. The numbers of total, deregulated and rescued genes in each class are shown. Box plots show the median and lower and upper quartiles, whiskers show the maximum and minimum data points up to 1.5 times the interquartile range.

d) Genomic view of inducible genes (grey), deregulated genes (blue) and rescue of gene expression by IFN-γ pre-treatment (green), assessed by fold-change and/or DESeq-2 analysis of RNA-seq data from control and *Rad21*$^{-/-}$ macrophages. 3 biological RNA-seq replicates.

Europe PMC Funders Author Manuscripts

Europe PMC Funders Author Manuscripts

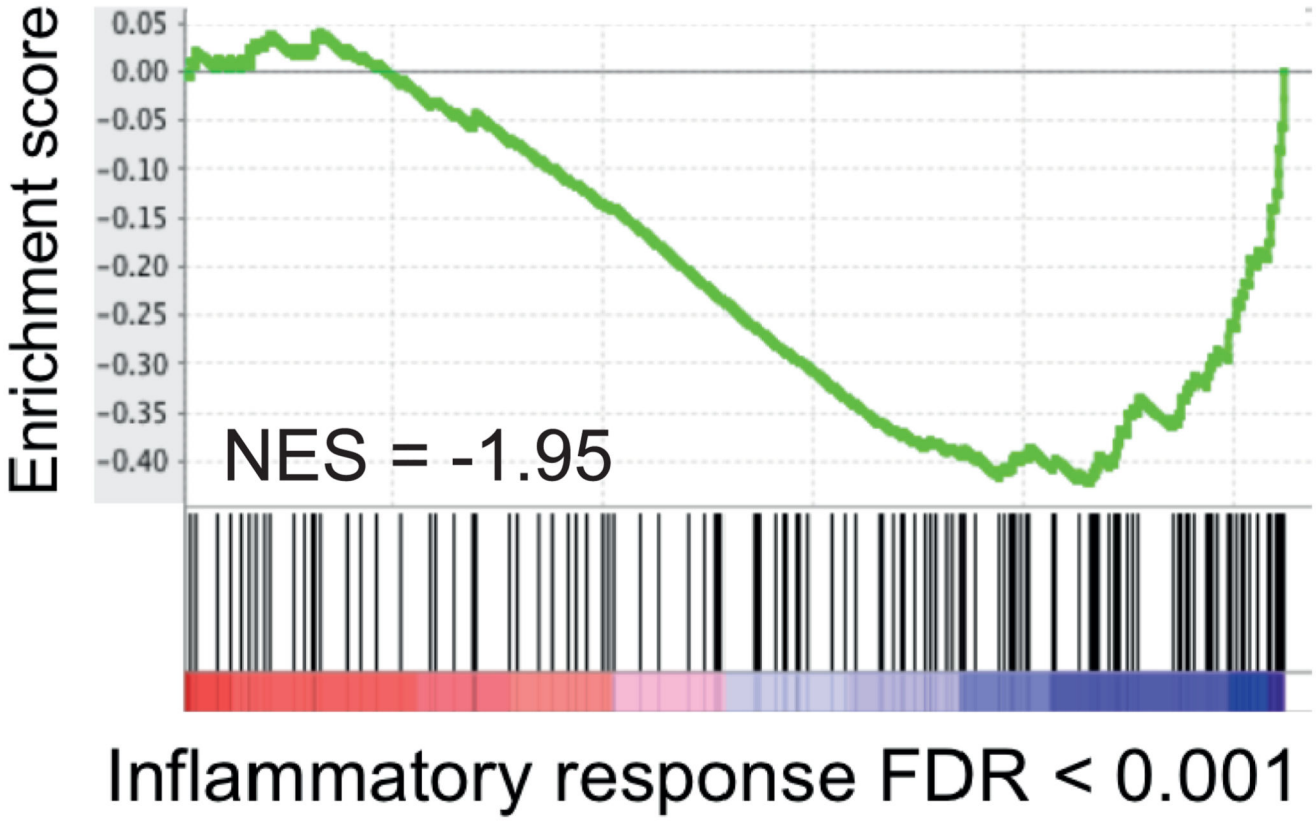

Figure 7. Cohesin controls inflammatory gene expression in HSPCs

GSEA analysis of inflammatory gene expression by HSPCs after *Stag2* versus control RNAi (FDR= 2.96E-4, data from ref. 31).

Europe PMC Funders Author Manuscripts

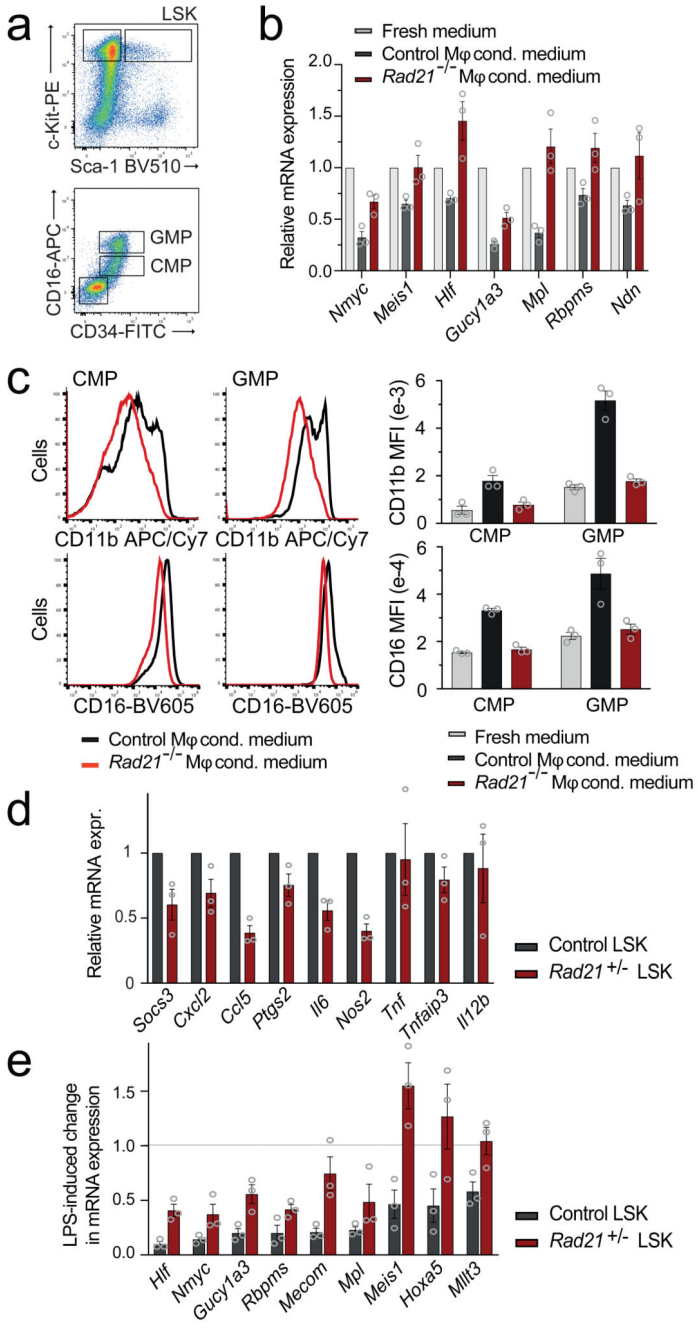

Figure 8. Cohesin controls the responsiveness of HSPCs to inflammatory stimuli.

a) Flow cytometric isolation of LSK, CMP and GMP populations.

b) RT-PCR analysis of stem cell gene expression in LSKs exposed for 48 h to media conditioned by LPS-pulsed wild-type or *Rad21*-deleted macrophages. Normalized to gene expression in fresh medium. Mean ± SE of 3 biological replicates. Comparisons between wild-type and *Rad21*-deleted macrophage conditioned medium were $P < 0.05$ for all genes except *Ndn* (*t*-test).

c) Flow cytometric analysis of the myeloid differentiation antigens CD11b and CD16 on CMPs and GMPs exposed to media conditioned by LPS-pulsed wild-type or *Rad21*-deleted macrophages for 48 h. MFI: mean fluorescence intensity. Mean ± SE of 3 biological replicates. Comparisons between wild-type and *Rad21*-deleted macrophage conditioned medium were $P < 0.05$ for CD11b and CD16 (two-sided *t*-test).

d) Quantitative RT-PCR analysis of inflammatory gene expression in $Rad21^{+/-}$ relative to wild-type LSK cells exposed to LPS for 8 h (mean ± SEM of 3 biological replicates, $P < 0.05$ for all genes except *Tnf*, *Tnfaip3* and *Il12b*, two-sided *t*-test). RAD21 expression in $Rad21^{+/-}$ bone marrow was 79% ± 8% of wild-type bone marrow (mean ± SEM of 4 biological replicates).

e) Quantitative RT-PCR analysis of stem cell gene expression in $Rad21^{+/-}$ relative to wild-type LSKs exposed to LPS for 8 h. Mean ± SEM of 3 biological replicates. *Hlf, Gucy1a3, Mecom, Meis1* and *Mllt3* were significantly higher in LPS-stimulated $Rad21^{+/-}$ than wild-type LSKs ($P < 0.05$, two-sided *t*-test). $P = 0.0014$ by two-sided *t*-test over all transcripts.

Europe PMC Funders Author Manuscripts

Table 1

Inducible enhancers with ISRE/IRF-PU.1 motifs are significantly more likely to fail than inducible enhancers with NF-κB or NFAT motifs.

P-value and odds ratios were determined by Fisher's exact test.

	Failed	Maintained
NFkB or NFAT motif	57	90
No NFkB or NFAT motif	161	139
P = 0.003, odds ratio = 0.55: Less likely to fail		

	Failed	Maintained
ISRE or IRF-PU1 motif	30	4
No ISRE or IRF-PU1 motif	188	225
P = 1 x 10-6, odds ratio = 8.94: More likely to fail		

Europe PMC Funders Author Manuscripts

Table 2

Genes downregulated in HSPCs with reduced cohesin function are upregulated in chronic inflammation.

Downregulated genes in HSPCs with reduced cohesin function (*31 versus 53; **32) were intersected with genes upregulated in chronic inflammation53. Gene ontology pathways enriched in the overlap were included 'Cytokine-mediated signaling pathway', 'Cellular response to IFN-γ', 'Cellular response to cytokine stimulus' and 'Regulation of cytokine production'.

Smc1 RNAi versus inflammation* Odds ratio 5.97, *P* = 2.4 x 10-8
Stag2 RNAi versus inflammation* Odds ratio 6.09, *P* = 1.9x 10-15
Smc3$^{+/-}$ versus inflammation** Odds ratio 8.49, *P* = 5.4 x 10-11
Combined: Odds ratio = 7.59, *P* = 5.9e-28